The green box: an electronically versatile perylene diimide macrocyclic host for fullerenes

Supporting Information

Timothy A. Barendt, William K. Myers, Stuart P. Cornes, Maria A. Lebedeva, Kyriakos Porfyrakis, Igor Marques, Vítor Félix and Paul D. Beer**

Contents page

1. Synthesis and characterisation S2
2. Further NMR spectroscopy data S12
3. Further mass spectrometry data S17
4. Photophysics S20
5. Electrochemistry S28
6. EPR spectroscopy S31
7. Kinetic data S35
8. Bindfit data S38
9. Free energy of electron transfer S42
10. Molecular modelling S43
11. References S47

1. Synthesis and Characterisation

All commercial solvents and reagents were used as purchased, unless otherwise stated. Anhydrous solvents were degassed with N_2 and dried by passing them through an MBraun-800 column. $Cu(MeCN)_4 \cdot PF_6$ was stored in a desiccator with P_2O_5. TBTA was prepared following a literature procedure.[1] Water was distilled and microfiltered using a Milli-Q Millipore machine. Chromatography was undertaken using silica gel (particle size: 40-63 μm) or preparative TLC plates (20 × 20 cm, 1 cm silica thickness).

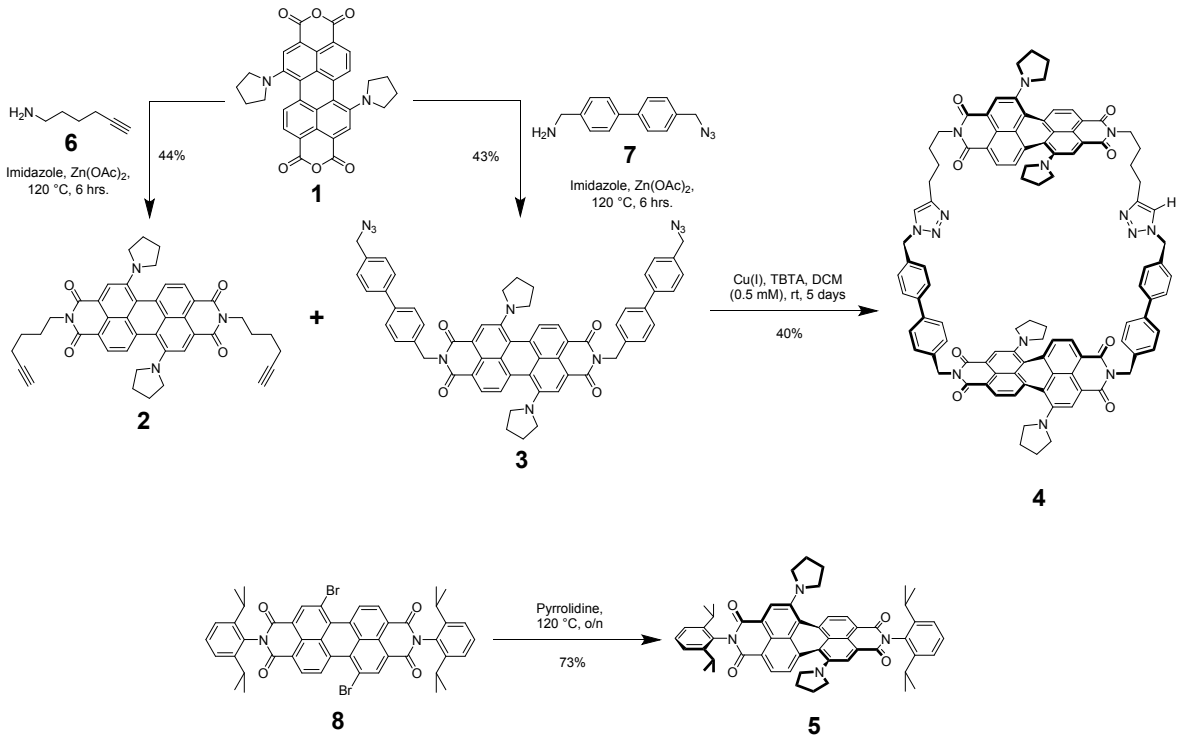
^1H and ^{13}C NMR spectra were recorded using Bruker AVIII400 (400 MHz) and Bruker AVIII500 (500 MHz, equipped with a ^{13}C detect cryoprobe) spectrometers. Mass spectra were recorded on Bruker MALDI Autoflex (MALDI-TOF MS) or Thermo Orbitrap Exactive MS (Waters Acquity Ultraperformance LC system HR ESI) mass spectrometers.

Details of equipment used in other characterisation techniques (EPR, photophysics, CV etc.) are provided in their appropriate sections in this supporting information.

The synthesis of compound **1** was achieved according to a literature procedure.[2] Importantly for bis-bay functionalised PDI compounds, the major C1,7 regioisomer was purified during the synthetic procedure courtesy of repetitive recrystallization from a 1:1 CH_2Cl_2:hexane solvent mixture similar to the procedure reported by Würthner *et al*.[3]

The syntheses of compounds **5**,[4] **6**,[5] **7**[6] and **8**[7] were also achieved according to literature procedures.

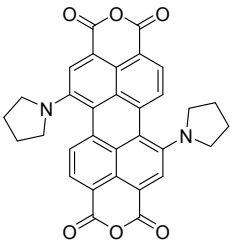
* = trace residual solvent



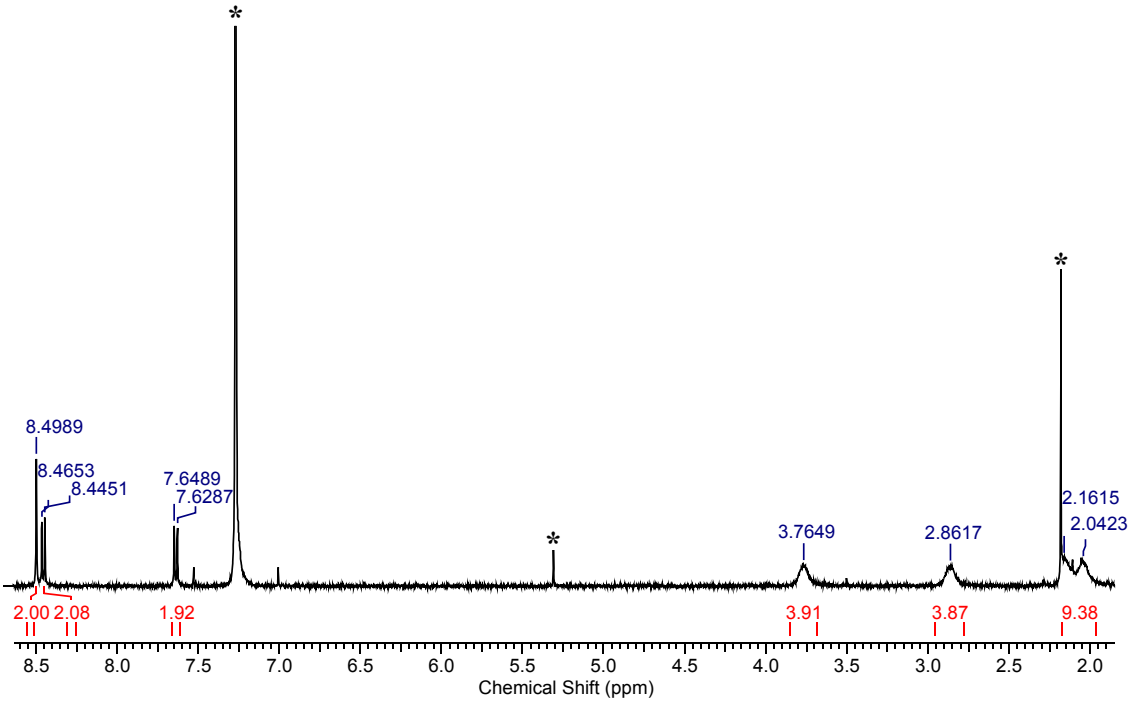
Scheme S1.1. Synthesis of the bis-PDI macrocycle "Green Box" **4** and bis-pyrrolidine PDI single panel **5**.

Bis-pyrrolidine perylene-3,4,9,10-tetracarboxylic dianhydride 1

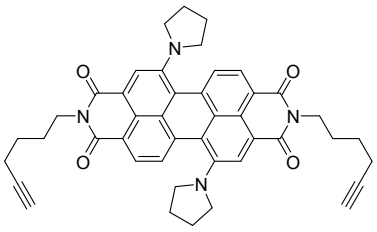
This compound was synthesised according to a literature procedure.[2]



^{1}H NMR (400MHz, $CDCl_3$) δ = 8.50 (2H, s, Ar*H* PDA), 8.45 (2H, d, *J* = 8.1 Hz, Ar*H* PDA), 7.64 (2H, d, *J* = 8.1 Hz, Ar*H* PDA), 3.76 (4H, br. s., CH_2 Py), 2.86 (4H, br. s., CH_2 Py), 2.16 (4H, br. s., CH_2 Py), 2.04 (4H, br. s., CH_2 Py)



Bis-butyl alkyne pyrrolidine PDI 2



A round bottom flask was charged with bis-pyrrolidine PDA **1** (100 mg, 0.19 mmol, 1 eq), hex-5-yn-1-amine **6** (91 mg, 0.95 mmol, 5 eq), $Zn(OAc)_2{\cdot}6H_2O$ (84 mg, 0.38 mmol, 2 eq) as a Lewis acid catalyst and imidazole (5 g) as solvent. The temperature was slowly increased and, upon melting of imidazole (~ 90°C), raised to 120 °C and the solution stirred for six hours under a flow of $N_{2\ (g)}$. After this time, heating was stopped and 1 M $HCl_{\ (aq)}$ (15 mL) was added gradually over five minutes under

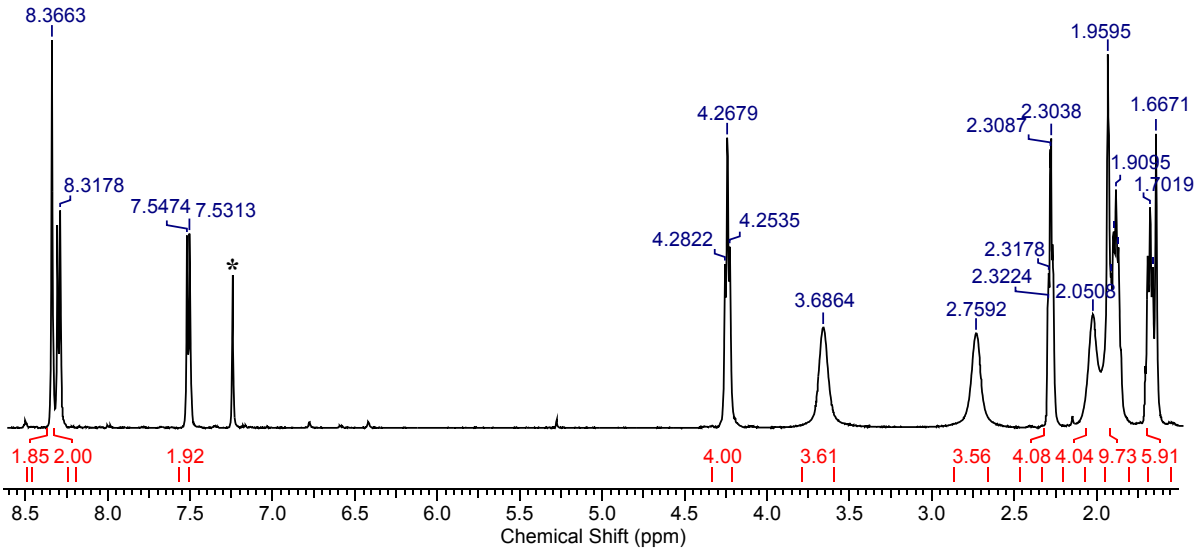
stirring to cause formation of a green precipitate. On cooling to room temperature this precipitate was collected by vacuum filtration, washed with H_2O until neutral pH and thoroughly dried in the oven and under vacuum. Silica gel column chromatography (50:45:5 $CHCl_3$:cyclohexane:acetone) was used to purify the desired bis-butyl alkyne pyrrolidine PDI **2** from the crude reaction mixture, isolated as a green solid (58 mg, 0.08 mmol, 44%).

^{1}H NMR (500MHz, $CDCl_3$) δ = 8.37 (2H, s, Ar*H* PDI), 8.33 (2H, d, *J* = 7.9 Hz, Ar*H* PDI), 7.54 (2H, d, *J* = 8.1 Hz, Ar*H* PDI), 4.27 (4H, t, *J* = 7.2 Hz, CH_2), 3.69 (4H, br. s., CH_2 Py), 2.76 (4H, br. s., CH_2 Py), 2.31 (4H, td, *J* = 6.9 Hz, ^4J = 2.3 Hz, CH_2), 2.05 (4H, br. s., CH_2 Py), 1.85 - 1.99 (8H, m, CH_2, CH_2 Py), 1.62 - 1.76 (6H, m, CH_2, C*H* alkyne)

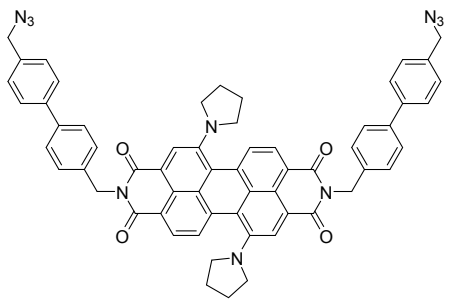
^{13}C NMR (126MHz, $CDCl_3$) δ = 164.0, 146.4, 134.1, 129.8, 126.6, 123.7, 122.0, 121.5, 120.7, 118.9, 117.9, 84.2, 68.5, 52.1, 39.8, 29.7, 27.4, 26.1, 25.8, 18.3

MS (MALDI): m/z calc. for $C_{44}H_{40}N_4O_4$ [M]: 688.304; found: 688.291

HRMS (ESI): m/z calc. for $C_{44}H_{41}N_4O_4$ $[M+H]^+$: 689.3122; found: 689.3129



Bis-biphenyl azide pyrrolidine PDI 3



A round bottom flask was charged with bis-pyrrolidine PDA **1** (100 mg, 0.19 mmol, 1 eq), biphenyl amine azide **7** (224 mg, 0.95 mmol, 5 eq), $Zn(OAc)_2 \cdot 6H_2O$ (84 mg, 0.38 mmol, 2 eq) as a Lewis acid catalyst and imidazole (5 g) as solvent. The temperature

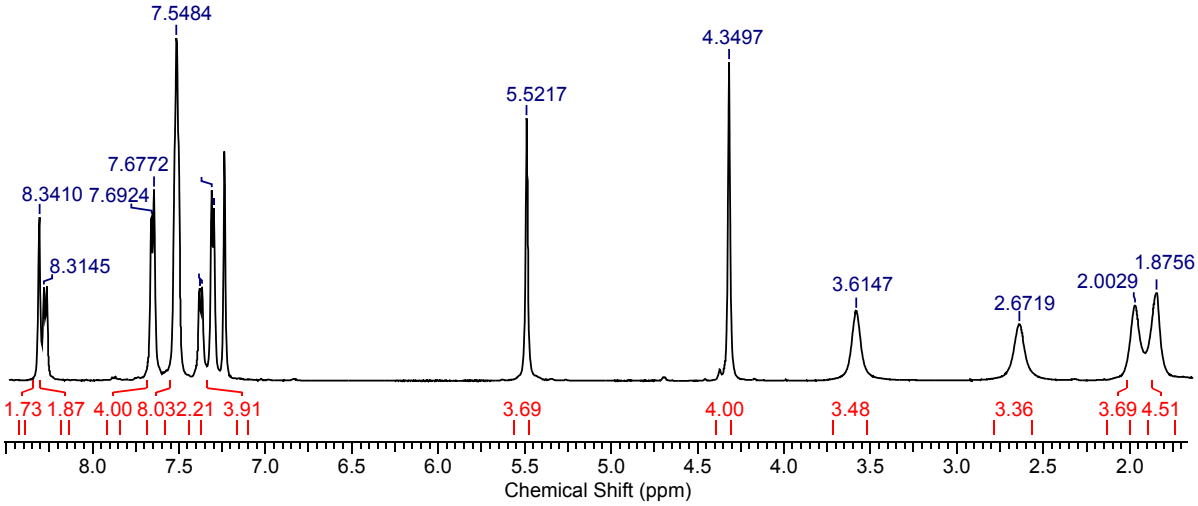
was slowly increased and, upon melting of imidazole (~ 90°C), raised to 120 °C and the solution stirred for six hours under a flow of $N_{2\ (g)}$. After this time, heating was stopped and 1 M $HCl_{\ (aq)}$ (15 mL) was added gradually over five minutes under stirring to cause formation of a green precipitate. On cooling to room temperature this precipitate was collected by vacuum filtration, washed with H_2O until neutral pH and thoroughly dried in the oven and under vacuum. Silica gel column chromatography (50:45:5 $CHCl_3$:cyclohexane:acetone) was used to purify the desired bis-biphenyl azide pyrrolidine PDI **3** from the crude reaction mixture, isolated as a green solid (79 mg, 0.08 mmol, 43%).

^{1}H NMR (500MHz, $CDCl_3$) δ = 8.34 (2H, s, Ar*H* PDI), 8.31 (2H, d, *J* = 7.8 Hz, Ar*H* PDI), 7.68 (4H, d, *J* = 7.6 Hz, Ar*H* biphenyl), 7.50 - 7.60 (8H, m, Ar*H* biphenyl), 7.41 (2H, d, *J* = 7.6 Hz, Ar*H* PDI), 7.34 (4H, d, *J* = 7.5 Hz, Ar*H* biphenyl), 5.52 (4H, s, C*H*$_2$), 4.35 (4H, s, C*H*$_2$), 3.61 (4H, br. s., C*H*$_2$ Py), 2.67 (4H, br. s., C*H*$_2$ Py), 2.00 (4H, br. s., C*H*$_2$ Py), 1.88 (4H, br. s., C*H*$_2$ Py)

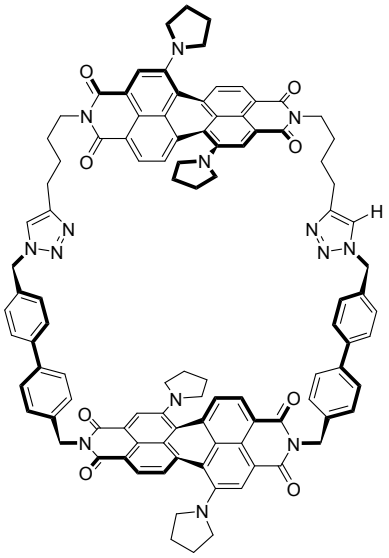
^{13}C NMR (126MHz, $CDCl_3$) δ = 163.9, 163.8, 146.2, 140.8, 139.4, 136.9, 134.2, 133.8, 129.5, 129.3, 128.5, 127.3, 127.0, 126.5, 123.5, 121.8, 121.3, 120.7, 118.7, 117.7, 54.4, 52.0, 43.3, 25.6

MS (MALDI): m/z calc. for $C_{60}H_{46}N_{10}O_4$ [M]: 970.370; found: 970.402

HRMS (ESI): m/z calc. for $C_{104}H_{87}N_{14}O_8$ $[M+H]^+$: 971.3782; found: 971.3787



Bis-PDI macrocycle 4 ("Green Box")



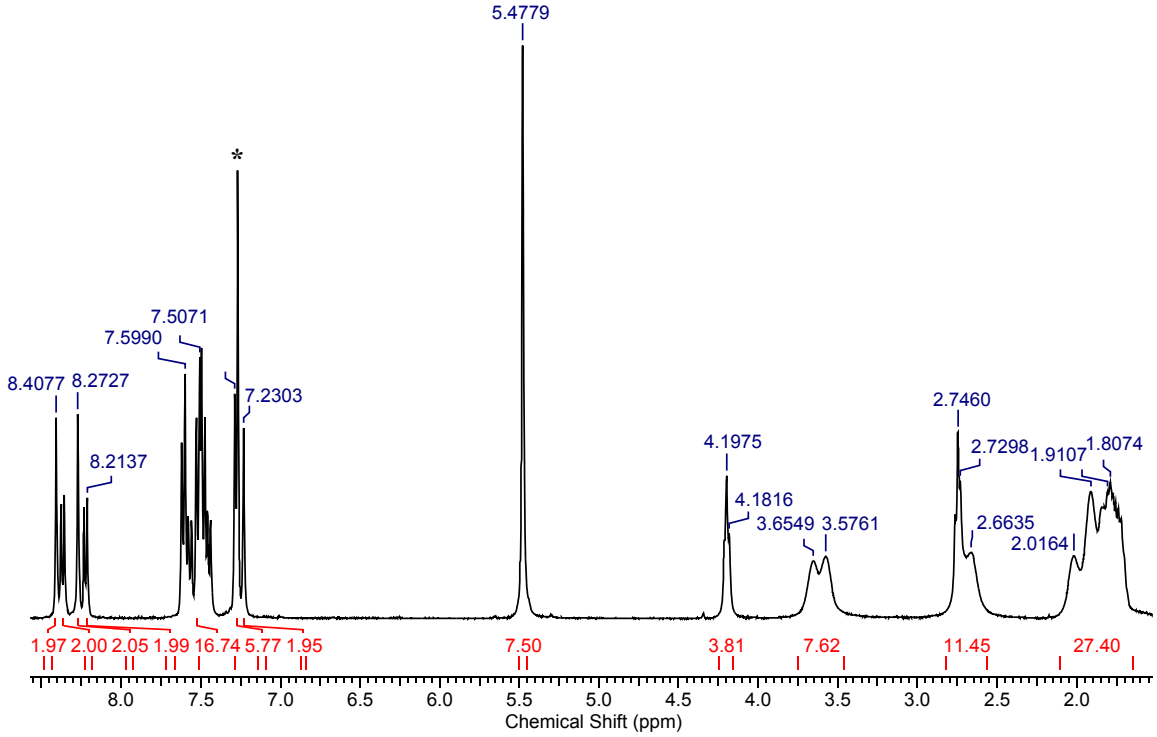
Under high-dilution conditions, bis-alkyne pyrrolidine PDI **2** (56 mg, 0.07 mmol, 1 eq) and bis-azide pyrrolidine PDI **3** (78 mg, 0.07 mmol, 1 eq) were dissolved in CH_2Cl_2 (140 mL) and TBTA (17 mg, 0.03 mmol, 0.4 eq) was added followed by $Cu(MeCN)_4 \cdot PF_6$ (12 mg, 0.03 mmol, 0.4 eq). The green solution was stirred at room temperature under an atmosphere of $N_{2\ (g)}$ for a minimum of five days with reaction progress monitored by thin-layer chromatography (97:3 CH_2Cl_2:MeOH). On depletion of all azide and alkyne starting materials the solvent was removed *in vacuo* and the crude mixture purified by iterative preparative silica thin-layer chromatography (CH_2Cl_2 to 98:2 CH_2Cl_2:MeOH) to yield bis-PDI macrocycle **4**, the "Green Box" as a dark green solid (46 mg, 0.02 mmol, 40%).

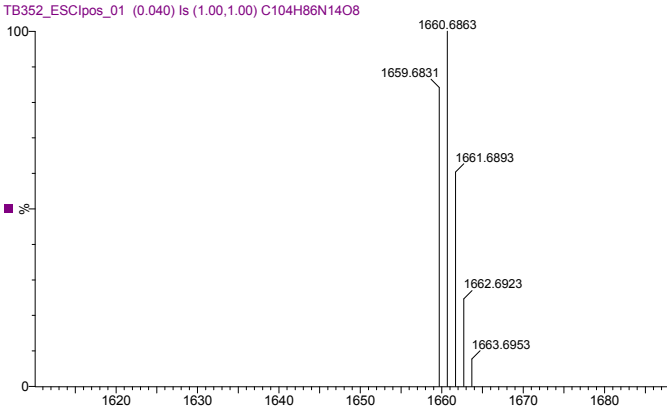
^{1}H NMR (400MHz, $CDCl_3$) δ = 8.41 (2H, s, Ar*H* PDI), 8.37 (2H, d, *J* = 8.1 Hz, Ar*H* PDI), 8.27 (2H, s, Ar*H* PDI), 8.22 (2H, d, *J* = 7.9 Hz, Ar*H* PDI), 7.61 (4H, d, *J* = 8.2 Hz, Ar*H* biphenyl), 7.57 (2H, d, *J* = 8.1 Hz, Ar*H* PDI), 7.52 (4H, d, *J* = 8.3 Hz, Ar*H* biphenyl), 7.49 (4H, d, *J* = 8.2 Hz, Ar*H* biphenyl), 7.45 (2H, d, *J* = 7.9 Hz, Ar*H* PDI), 7.28 (4H, d, *J* = 7.8 Hz, Ar*H* biphenyl), 7.23 (2H, s, Ar*H* triazole), 5.48 (8H, s, CH_2), 4.20 (4H, t, *J* = 7.1 Hz, CH_2), 3.65 (4H, br. s., CH_2 Py), 3.58 (4H, br. s., CH_2 Py), 2.70 - 2.82 (8H, m, CH_2, CH_2 Py), 2.66 (4H, br. s., CH_2 Py), 2.02 (4H, br. s., CH_2 Py), 1.65 - 1.98 (20H, m, CH_2, CH_2 Py)

^{13}C NMR (101MHz, $CDCl_3$) δ = 164.0, 163.9, 148.2, 146.4, 146.2, 141.2, 139.3, 137.0, 134.1, 134.0, 133.6, 129.8, 129.7, 129.4, 128.5, 127.6, 127.1, 126.7, 126.4, 123.9, 123.5, 122.0, 121.9, 121.6, 121.4, 120.9, 120.8, 120.5, 118.8, 118.8, 118.0, 117.8, 53.6, 52.0, 43.2, 39.8, 27.7, 26.8, 25.7, 25.6, 25.4

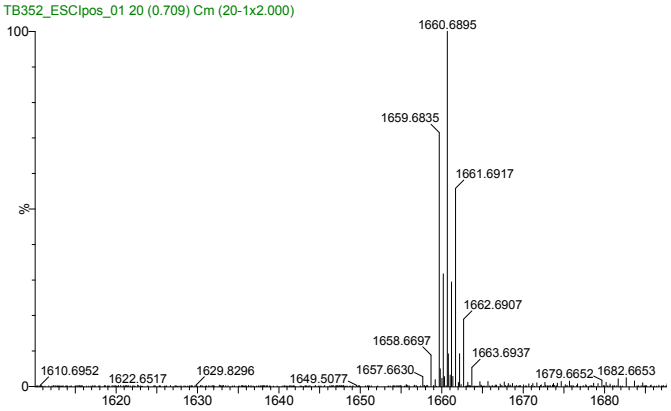
MS (MALDI): m/z calc. for $C_{104}H_{86}N_{14}O_8$ [M]: 1659.678; found: 1659.668 (see Section 3)

HRMS (ESI): m/z calc. for $C_{104}H_{87}N_{14}O_8$ $[M+H]^+$: 1660.6863; found: 1660.6895 (see below)



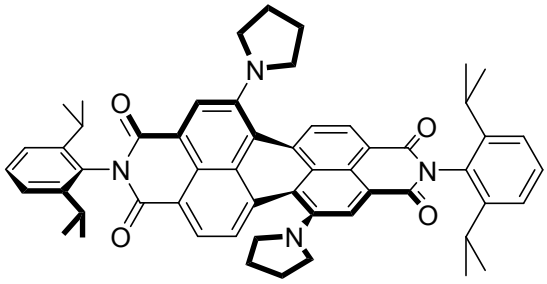


Calculated $[M+H]^+$



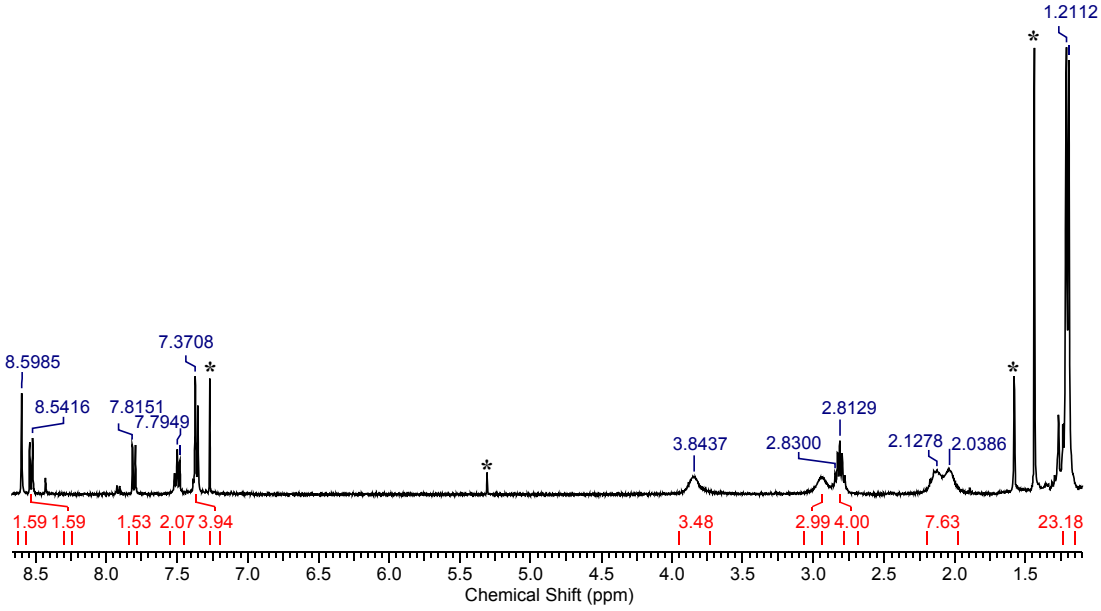
Found $[M+H]^+$

Bis-pyrrolidine PDI single panel 5

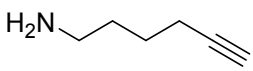


This compound was synthesised according to a literature procedure.[4]

^{1}H NMR (400MHz, $CDCl_3$) δ = 8.60 (2H, s, Ar*H* PDI), 8.53 (2H, d, *J* = 8.0 Hz, Ar*H* PDI), 7.80 (2H, d, *J* = 8.0 Hz, Ar*H* PDI), 7.50 (2H, t, *J* = 7.7 Hz, Ar*H* mes.), 7.36 (4H, d, *J* = 7.8 Hz, Ar*H* mes.), 3.84 (4H, br. s., CH_2 Py), 2.94 (4H, br. s., CH_2 Py), 2.81 (4H, spt, *J* = 7.2 Hz, CH mes.), 2.14 (4H, br. s, CH_2 Py), 2.04 (4H, br. s., CH_2 Py), 1.21 (12H, s, CH_3), 1.19 (12H, s, CH_3)

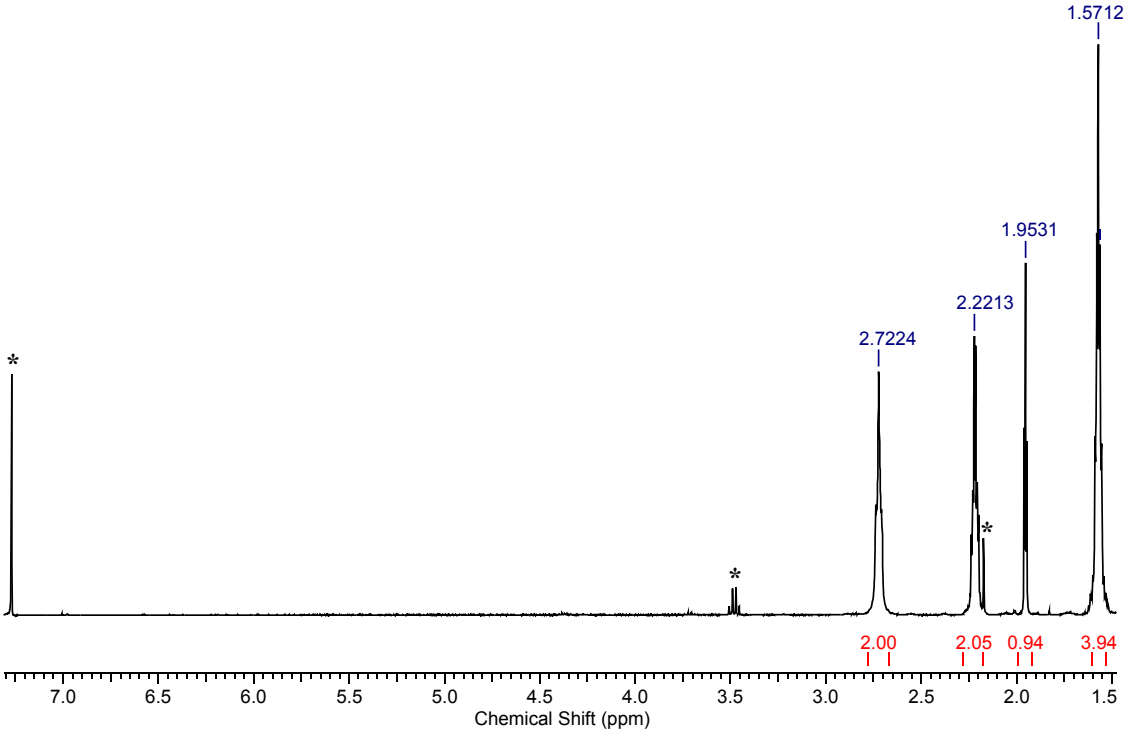


Hex-5-yn-1-amine 6

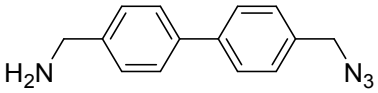


This compound was synthesised according to a literature procedure.[5]

^{1}H NMR (400MHz, $CDCl_3$) δ = 2.72 (2H, t, *J* = 6.5 Hz, CH_2), 2.17 - 2.28 (2H, m, CH_2), 1.95 (1H, t, *J* = 2.6 Hz, C*H* alkyne), 1.53 - 1.61 (4H, m, CH_2)

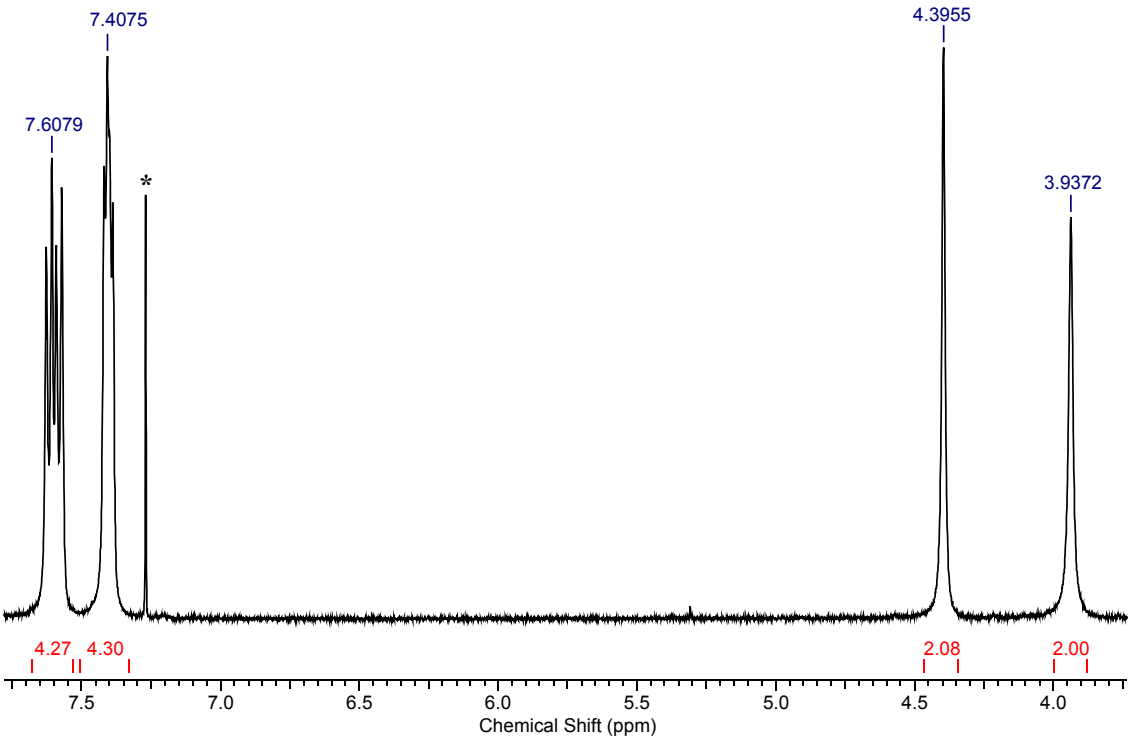


Biphenyl amine azide 7

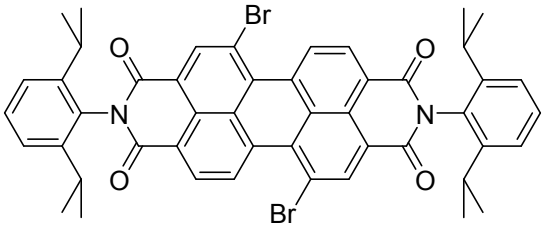


This compound was synthesised according to a literature procedure.[6]

^{1}H NMR (400MHz, $CDCl_3$) δ = 7.58 (2H, d, *J* = 8.1 Hz, Ar*H* biphenyl), 7.62 (2H, d, *J* = 8.1 Hz, Ar*H* biphenyl), 7.33 - 7.50 (4H, m, Ar*H* biphenyl), 4.40 (2H, s, CH_2), 3.94 (2H, s, CH_2)

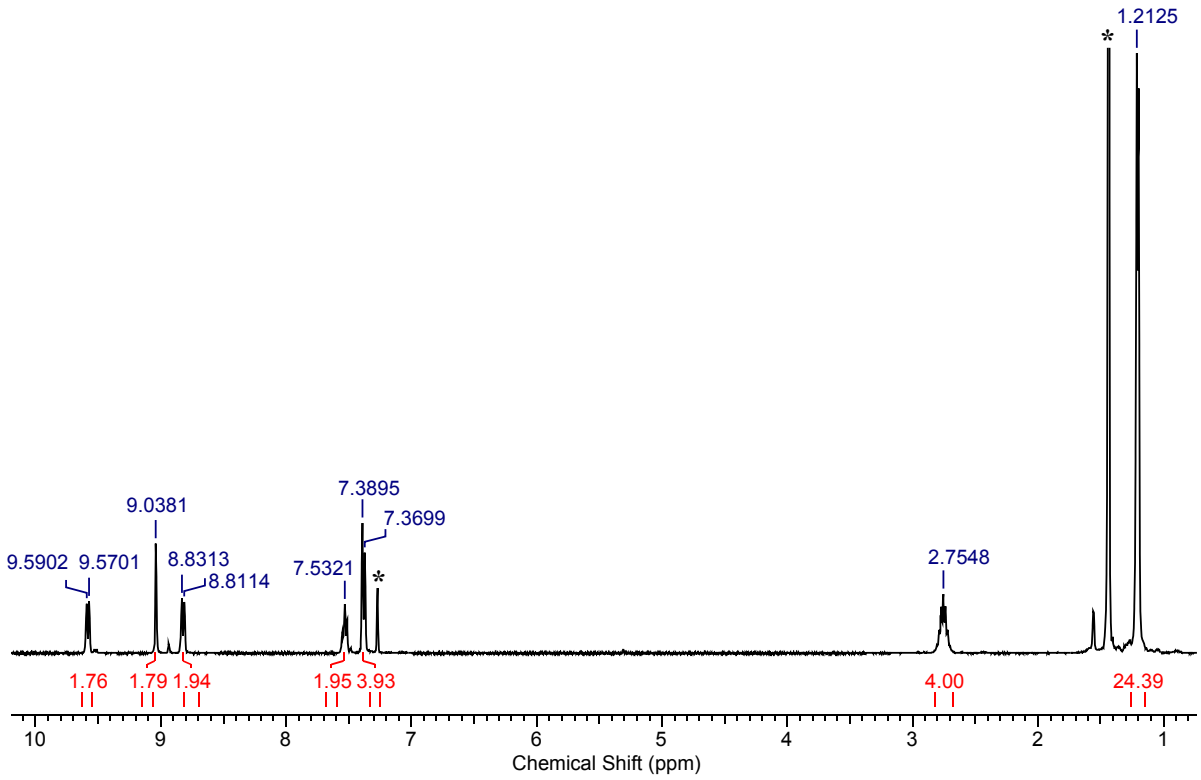


Bis-bromo mesityl PDI 8



This compound was synthesised according to a literature procedure.[7]

^{1}H NMR (400MHz, $CDCl_3$) δ = 9.58 (2H, d, *J* = 8.1 Hz, Ar*H* PDI), 9.04 (2H, s, Ar*H* PDI), 8.82 (2H, d, *J* = 7.9 Hz, Ar*H* PDI), 7.53 (2H, t, *J* = 7.8 Hz, Ar*H* mes.), 7.38 (4H, d, *J* = 7.8 Hz, Ar*H* mes.), 2.75 (4H, spt, *J* = 7.2 Hz, Ar*H* mes.), 1.21 (12H, s, CH_3), 1.20 (12H, s, CH_3)


1.2125
*
9.0381
7.3895
7.3699
9.5902
9.5701
8.8313
8.8114
7.5321
*
2.7548
1.76
1.79
1.94
1.95
3.93
4.00
24.39
10
9
8
7
6
5
4
3
2
1
Chemical Shift (ppm)

2. Further NMR spectroscopy data

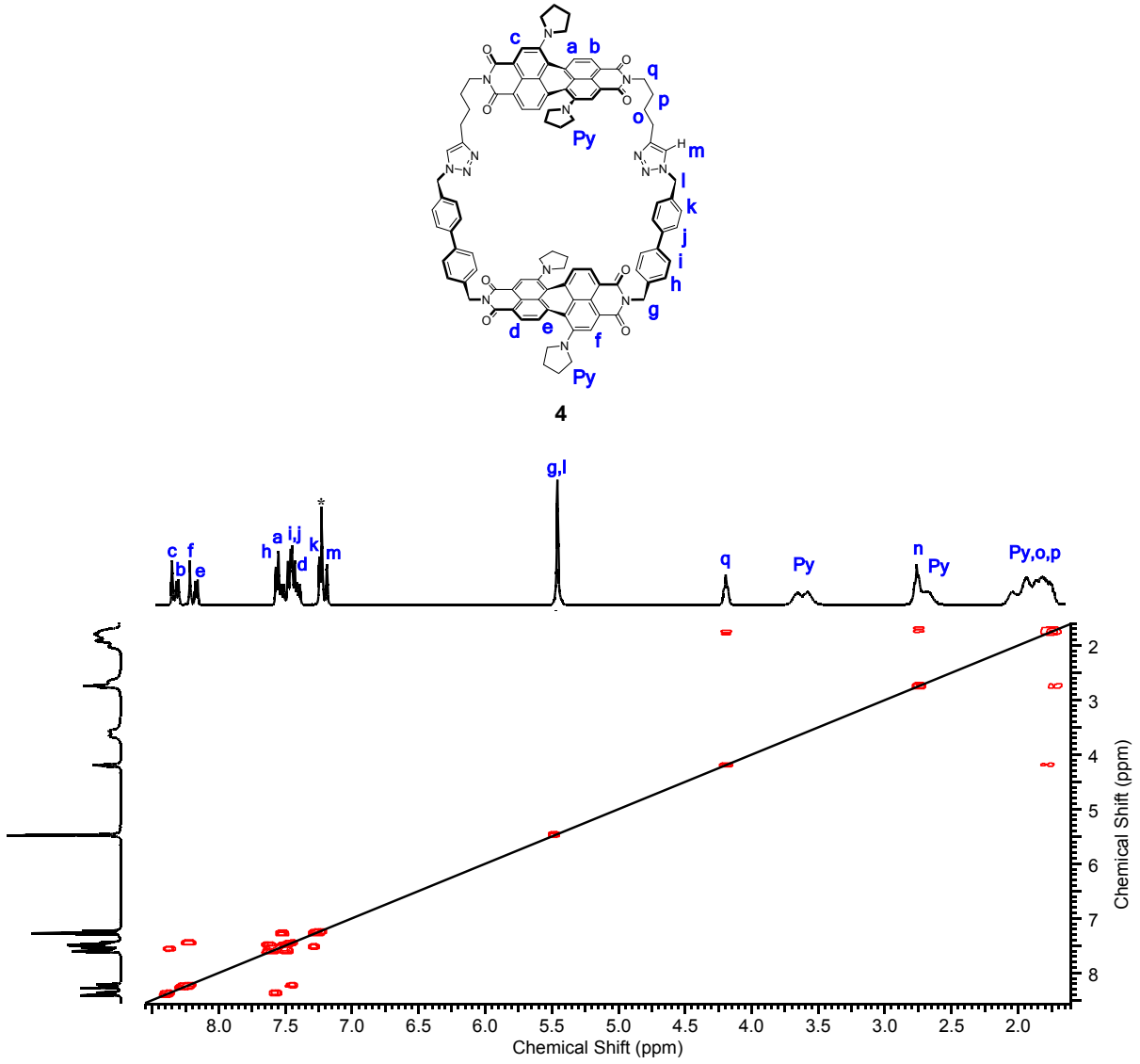


Figure S2.1. ^{1}H–^{1}H COSY NMR spectrum of Green Box **4** ($CDCl_3$, 298 K, 500 MHz).

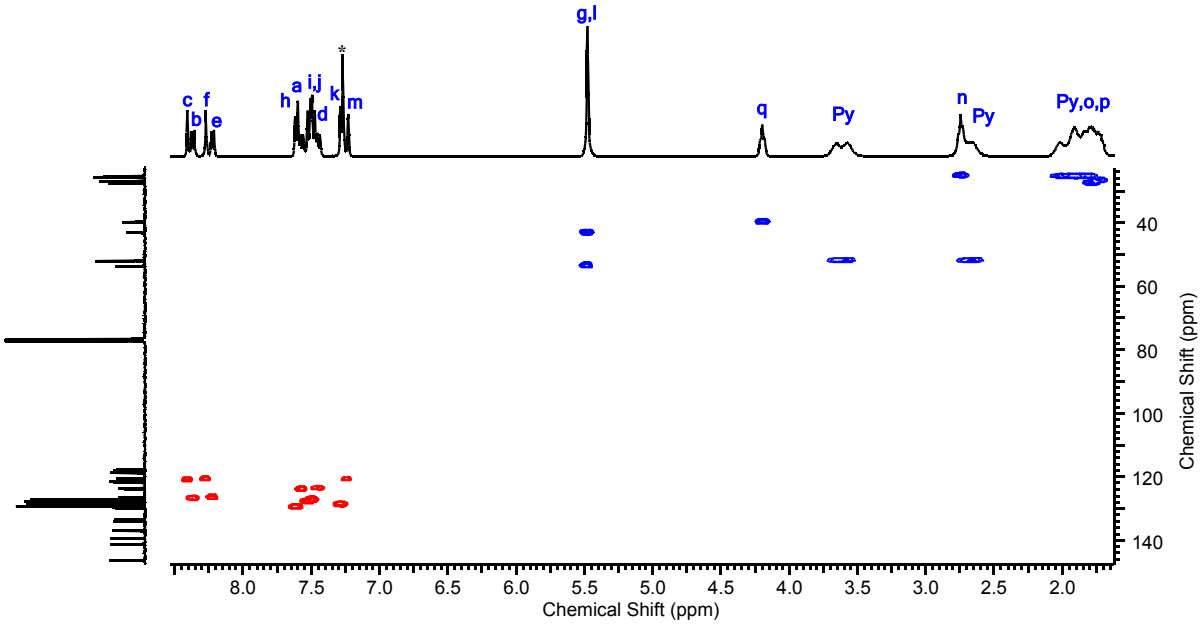


Figure S2.2. $^{1}H–^{13}C$ HSQC NMR spectrum of Green Box **4** ($CDCl_3$, 298 K, 500 MHz).

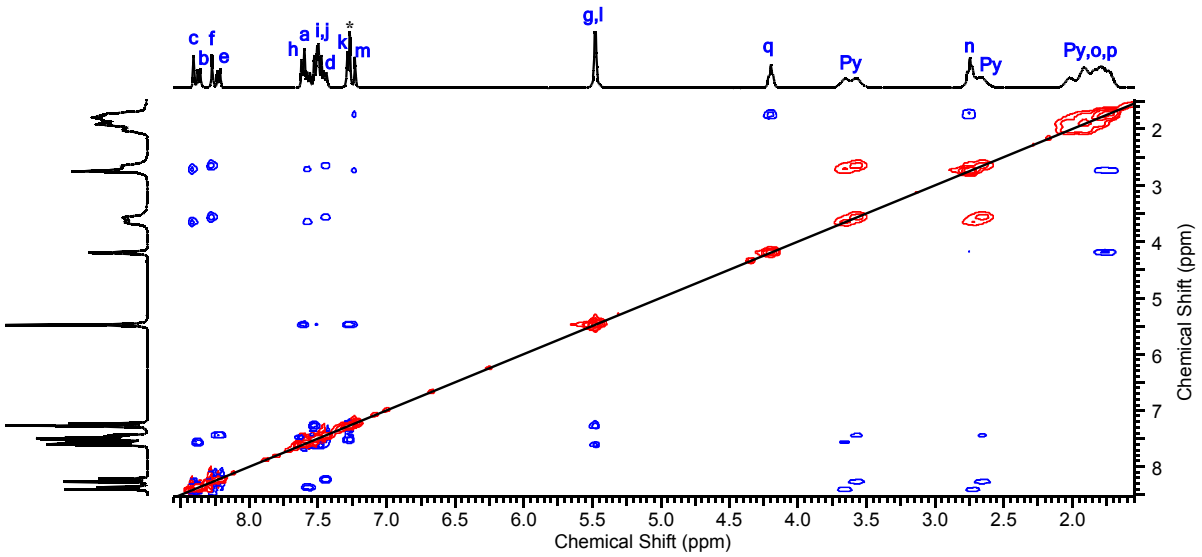


Figure S2.3. $^{1}H–^{1}H$ ROESY NMR spectrum of Green Box **4** ($CDCl_3$, 298 K, 500 MHz).

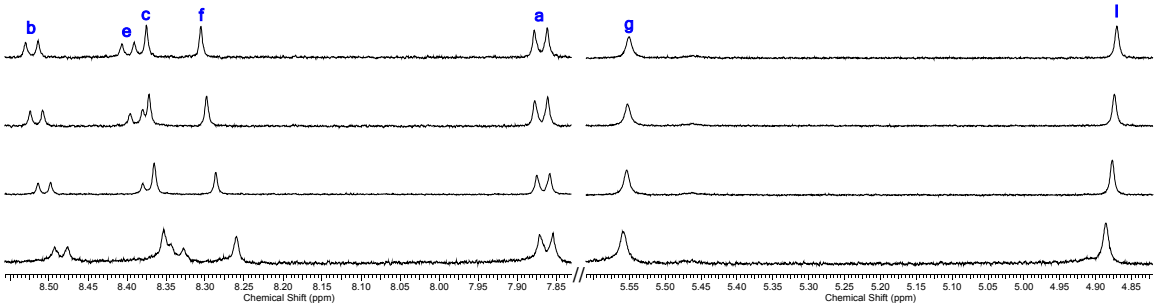


Figure S2.4. Truncated ^{1}H NMR spectra of Green Box **4** (0.4 mM) upon titration with up to three equivalents of C_{60} fullerene (d_8-toluene, 298 K, 500 MHz).

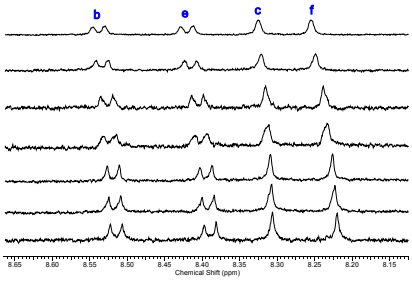


Figure S2.5. Truncated ^{1}H NMR spectra of Green Box **4** (0.4 mM) upon titration with up to 30 equivalents of C_{60} fullerene (d_4-o-DCB, 298 K, 500 MHz).

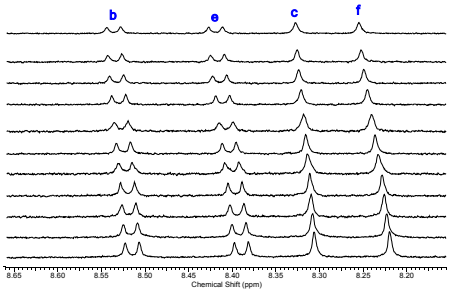


Figure S2.6. Truncated ^{1}H NMR spectra of Green Box **4** (0.4 mM) upon titration with up to 30 equivalents of C_{70} fullerene (d_4-o-DCB, 298 K, 500 MHz).

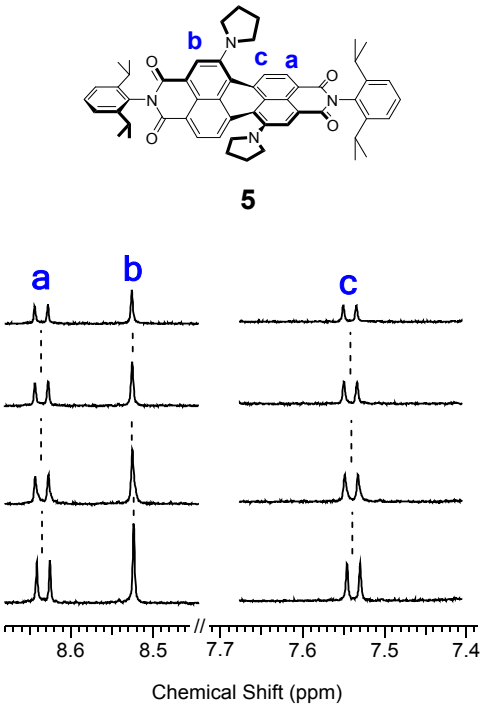


Figure S2.7. Truncated ^{1}H NMR spectra of bis-pyrrolidine PDI single panel **5** (0.4 mM) upon titration with up to three equivalents of C_{60} fullerene (d_8-toluene, 298 K, 500 MHz).

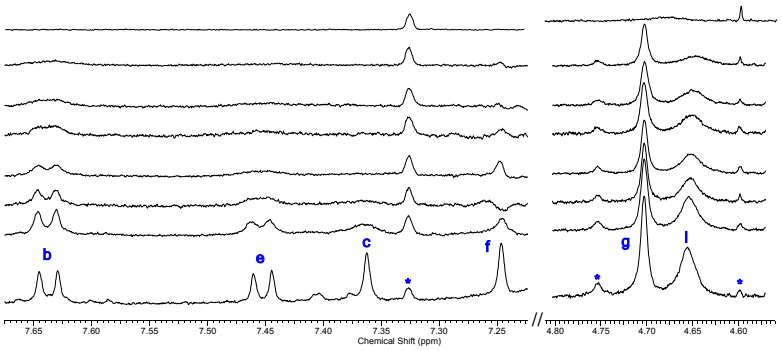


Figure S2.8. Truncated ^{1}H NMR spectra of Green Box **4** (0.4 mM) upon titration with up to one equivalent of C_{60} fullerene (d_5-nitrobenzene, 298 K, 500 MHz). * refers to inherent impurities from the deuterated solvent.

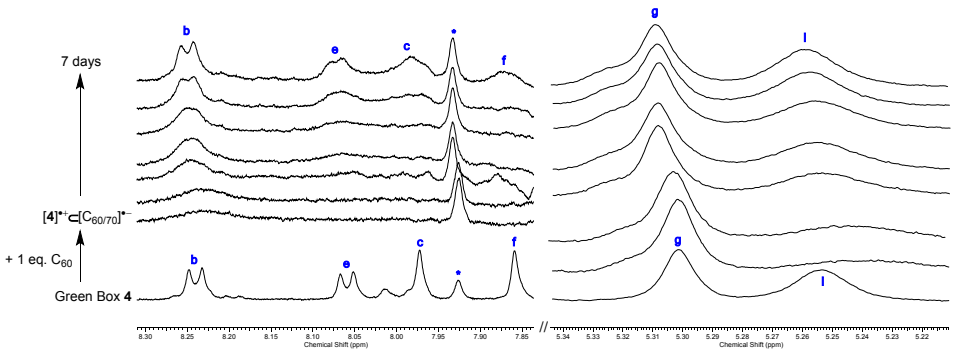


Figure S2.9. Truncated ^{1}H NMR spectra of Green Box–C_{60} fullerene complex [**4**]$^{\cdot+}$⊃[C_{60}]$^{\cdot-}$ (0.4 mM) recorded over seven days showing a gradual sharpening of peaks as radical concentration is depleted (d_5-nitrobenzene, 298 K, 500 MHz). * refers to inherent impurities from the deuterated solvent. Note that proton resonances in the complex are upfield shifted relative to Green Box in the absence of fullerene guest.

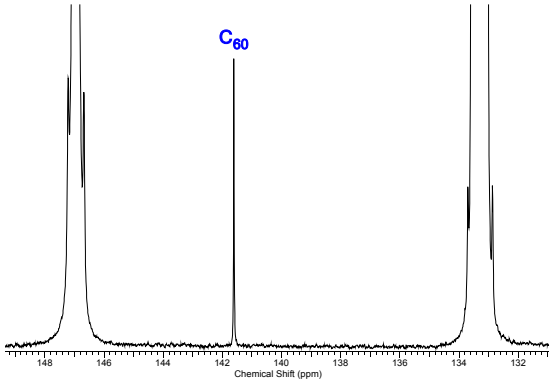


Figure S2.10. ^{13}C NMR spectrum of Green Box–C_{60} fullerene complex [**4**]$^{\cdot+}$⊃[C_{60}]$^{\cdot-}$ (0.4 mM) after seven days showing the presence of C_{60} fullerene in solution (d_5-nitrobenzene, 298 K, 101 MHz). Note there is negligible decomposition since any functionalisation causes desymmetrisation of the cage and appearance of multiple new resonances in this region of the ^{13}C NMR spectrum.

3. Further mass spectrometry data

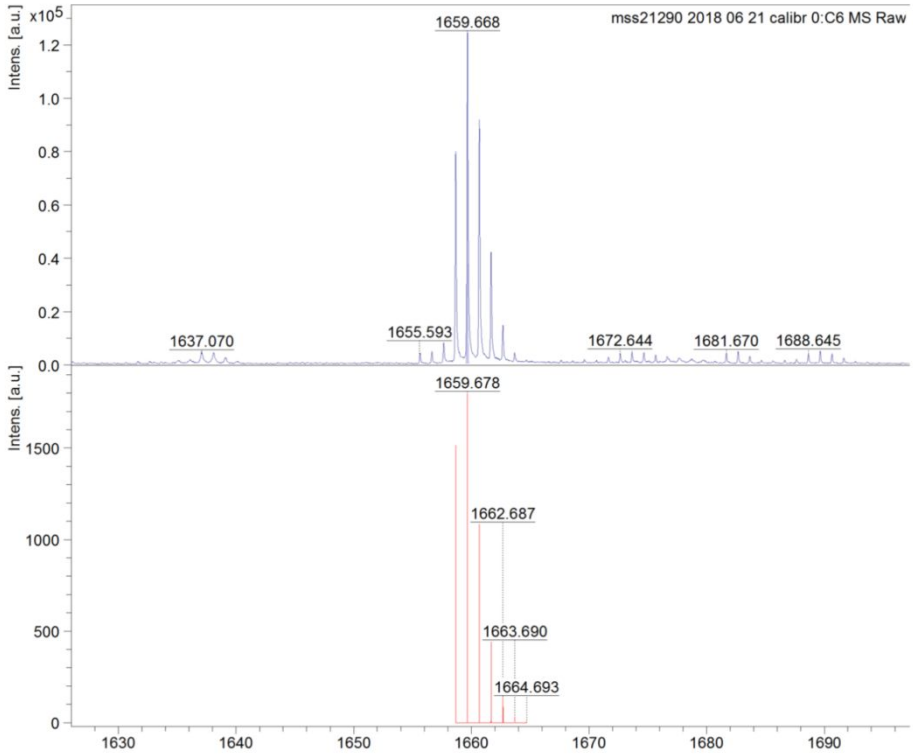


Figure S3.1. Theoretical (bottom) and measured (top) MALDI-TOF mass spectra of Green Box **4** (dithranol matrix).

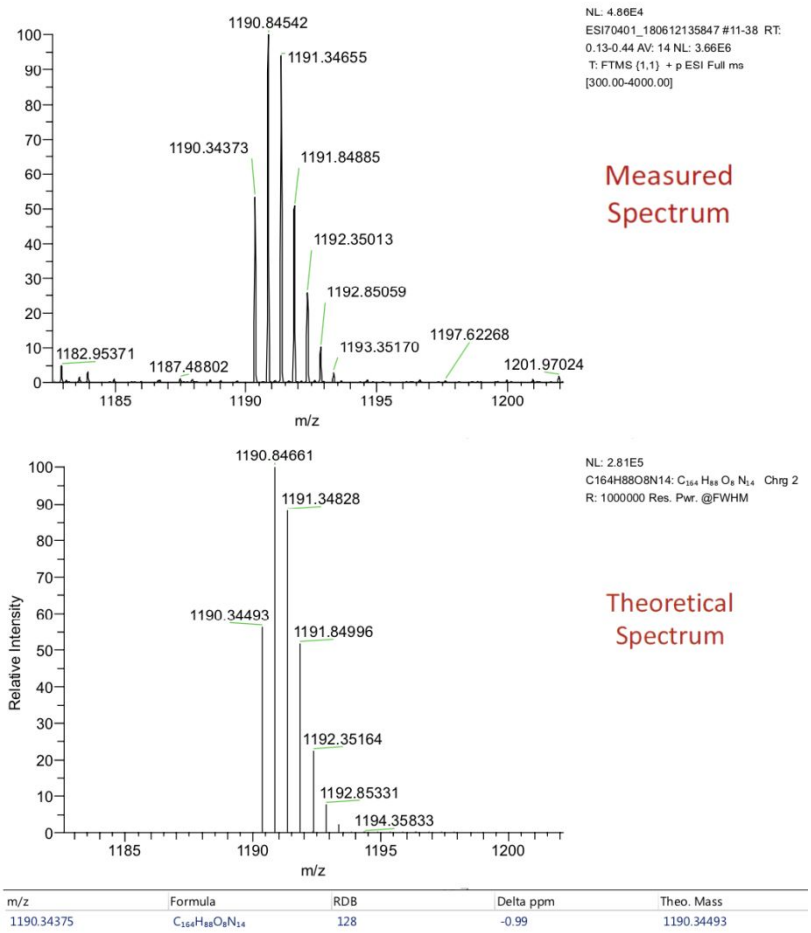


Figure S3.2. Theoretical (bottom) and measured (top) ESI mass spectra of Green Box–C_{60} fullerene complex [**4**]⊃[C_{60}] (m/z = [**4**+C_{60}+2H]$^{2+}$).

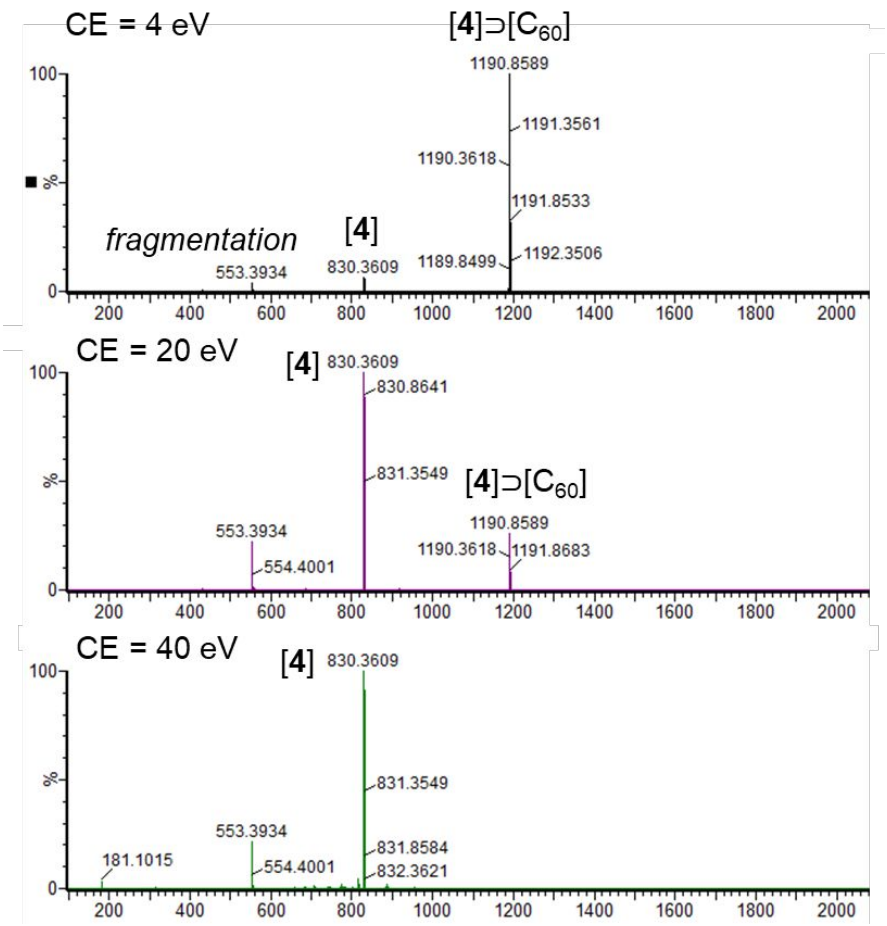


Figure S3.3. The ESI MS/MS spectrum of [**4**]⊃[C_{60}] as the complex is broken into its constituent parts upon increasing collision energy (CE, eV).

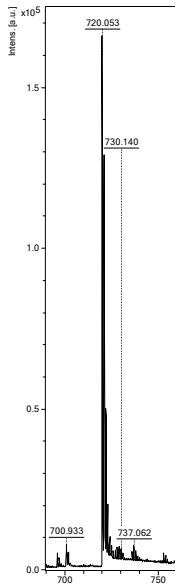


Figure S3.4. MALDI-TOF mass spectrum of Green Box–C_{60} fullerene complex [**4**]$^{\cdot+}$⊃[C_{60}]$^{\cdot-}$ after seven days showing the presence of C_{60} fullerene (m/z = 720) and negligible decomposition products (dithranol matrix).

4. Photophysics

a) Data

All steady state electronic absorption and emission spectra were recorded at a concentration of 1 x 10^{-5} M (unless otherwise stated) at 298 K. For UV-Vis-NIR spectroscopy a Jasco V-780 or a PGT60 U spectrophotometers were used. For fluorescence spectroscopy a Horiba Fluorolog 3 was used. Quartz cuvettes with 1 cm path length were used. For PDI host–fullerene guest titration spectra; [**4**] is kept constant, red line = start point, blue line = end point and absorption spectra have been corrected for fullerene absorbances unless otherwise stated.

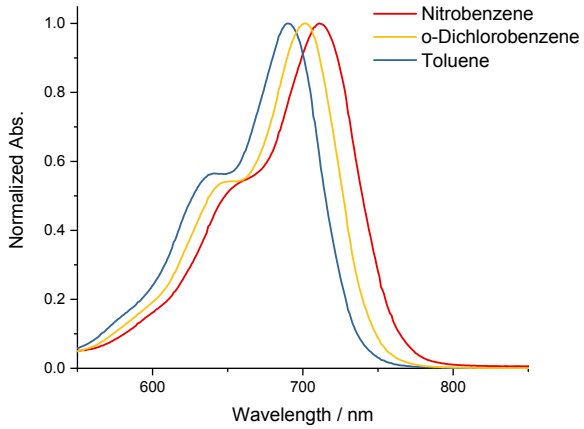


Figure S4.1. Normalized Vis-NIR absorption spectra of Green Box **4** recorded in aromatic solvents of differing polarity. Solvatochromism arises from the charge transfer character of the $S_0 \rightarrow S_1$ transition (λ_{max} = 689 - 712 nm).

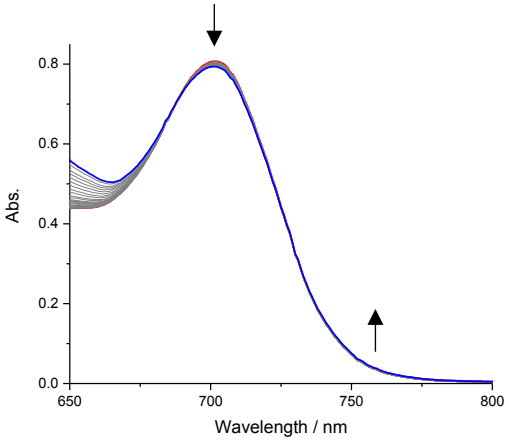


Figure S4.2. Uncorrected Vis-NIR absorption spectra of Green Box **4** upon the titration of 170 equiv. of C_{60} in o-DCB.

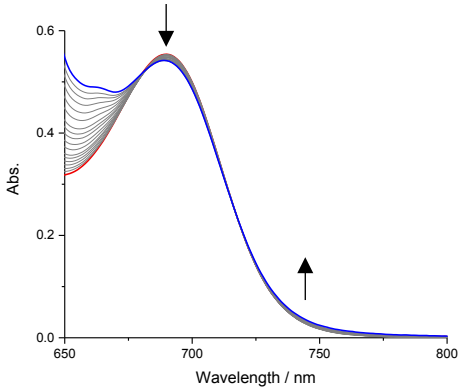


Figure S4.3. Uncorrected Vis-NIR absorption spectra of Green Box **4** upon the titration of 30 equiv. of C_{70} in toluene.

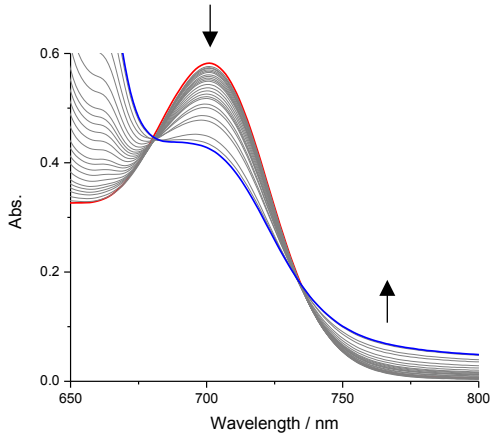


Figure S4.4. Uncorrected Vis-NIR absorption spectra of Green Box **4** upon the titration of 80 equiv. of C_{70} in o-DCB.

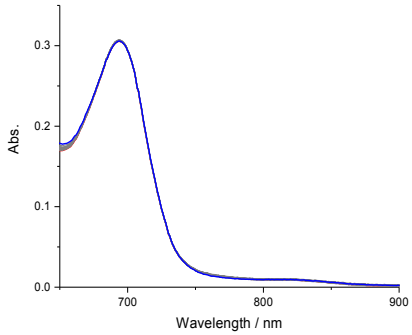


Figure S4.5. Vis-NIR absorption spectra of bis-pyrrolidine PDI single panel **5** upon the titration of 170 equiv. of C_{60} in toluene. Spectra changes are negligible in comparison to Green Box **4**.

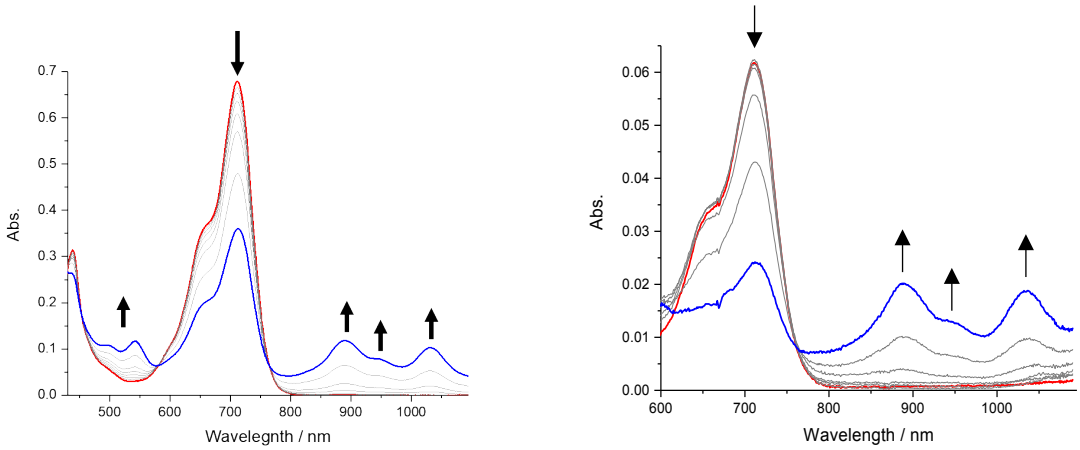


Figure S4.6. Vis-NIR absorption spectra of Green Box (left [**4**] = 10^{-5} M, right [**4**] = 10^{-6} M) upon the titration of 1.5 equiv. of C_{60} in nitrobenzene (spectra corrected for C_{60} absorptions), forming the 1:1 host–guest stoichiometric complex [**4**]⊃[C_{60}], χ ([**4**]⊃[C_{60}]) = 1.

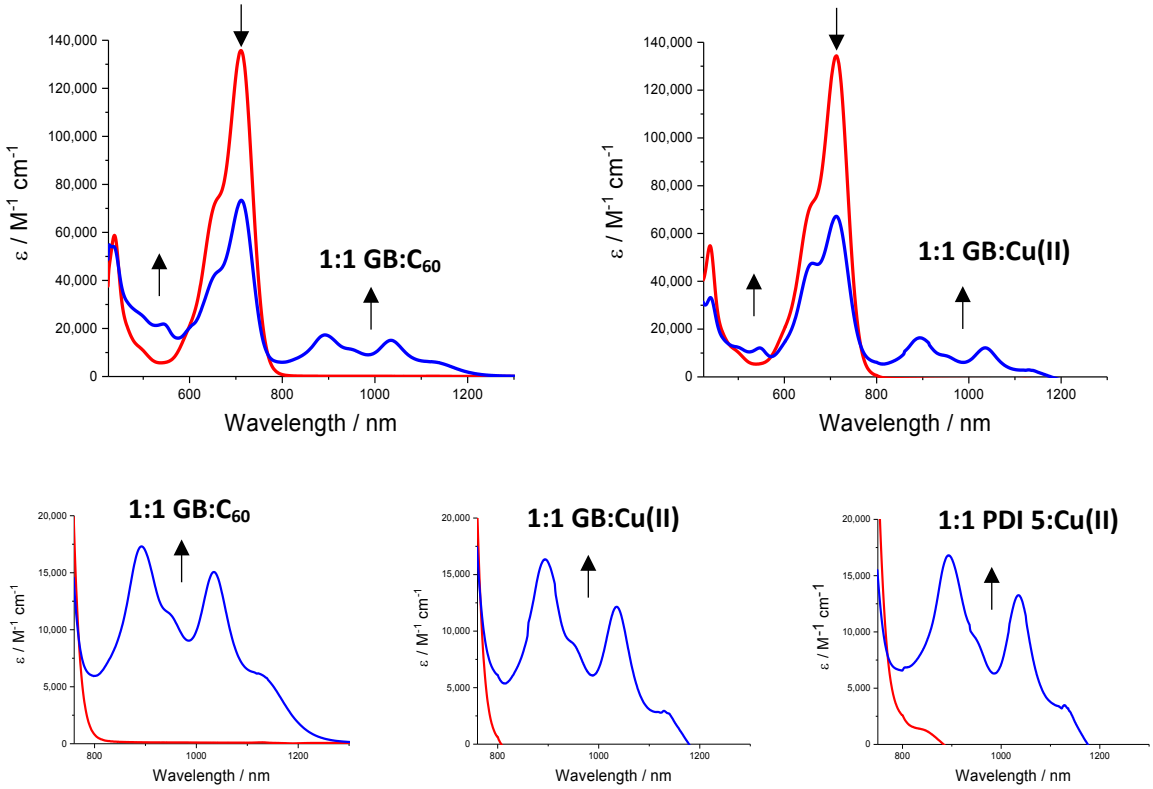


Figure S4.7. Comparative electronic absorption spectra (zoomed NIR regions below) of the 1:1 host–guest stoichiometric complex **4** ⊃ C_{60} and mixtures of **4**:Cu(II) triflate and single panel PDI **5**:Cu(II) triflate in nitrobenzene (blue lines). With both C60 and Cu(II), a near 50% decrease in intensity of the main PDI absorption band (S0→S1 transition, $\lambda_{abs,max}$ = 712 nm) indicates the stoichiometric oxidation of a single PDI unit. For reference, red lines = Green Box (GB) **4** in the absence of fullerene.

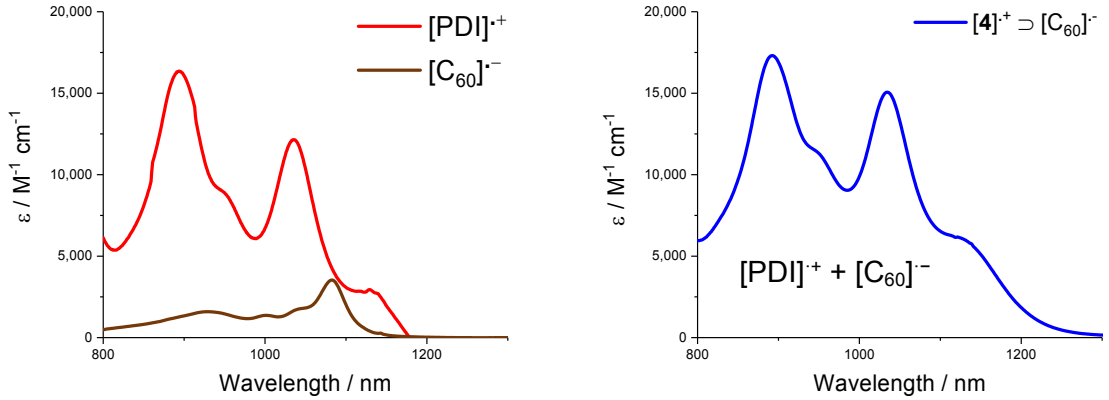


Figure S4.8. Vis-NIR electronic absorption spectra of chemically generated $[PDI]^{\cdot+}$ and $[C_{60}]^{\cdot-}$ species (left) and the Green Box–fullerene radical ion pair complex $[\mathbf{4}]^{\cdot+}\supset[C_{60}]^{\cdot-}$ (right) showing that the latter is a superposition of the former i.e. $[PDI]^{\cdot+} + [C_{60}]^{\cdot-} = [\mathbf{4}]^{\cdot+}\supset[C_{60}]^{\cdot-}$. All spectra collected in nitrobenzene except $[C_{60}]^{\cdot-}$ which is in benzonitrile. $[PDI]^{\cdot+}$ generated from **4** with one equivalent of Cu(II) triflate, $[C_{60}]^{\cdot-}$ generated from C_{60} with one equivalent of cobaltocene.[8] Relative to $[\mathbf{4}]^{\cdot+}\supset[C_{60}]^{\cdot-}$ in nitrobenzene, a small perturbation to the $[C_{60}]^{\cdot-}$ absorption band in $[Cp_2Co]^{\cdot+}\cdot[C_{60}]^{\cdot-}$ in benzonitrile is expected due to, a) its complexation and, b) the change in solvent.

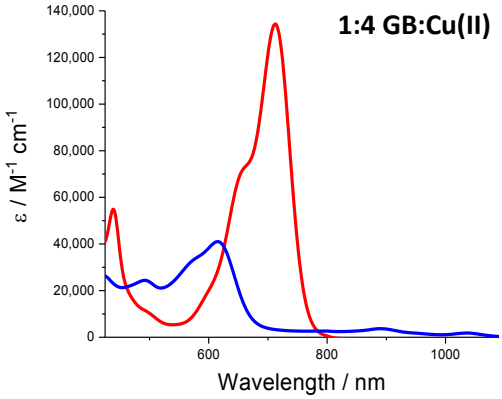


Figure S4.9. Vis-NIR electronic absorption spectrum of 1:4 stoichiometric mixture of Green Box **4**:Cu(II) triflate in nitrobenzene reveals diagnostic peaks (λ = 490, 614 nm) for the doubly oxidized bis-pyrrolidine PDI species.[9] These absorbances (i.e. λ_{max} = 614 nm) are not present in the 1:1 host–guest stoichiometric complex $[\mathbf{4}]\supset[C_{60}]$ (Figure S4.6), indicating only a single electron transfer (SET) process occurs between Green Box and fullerene.

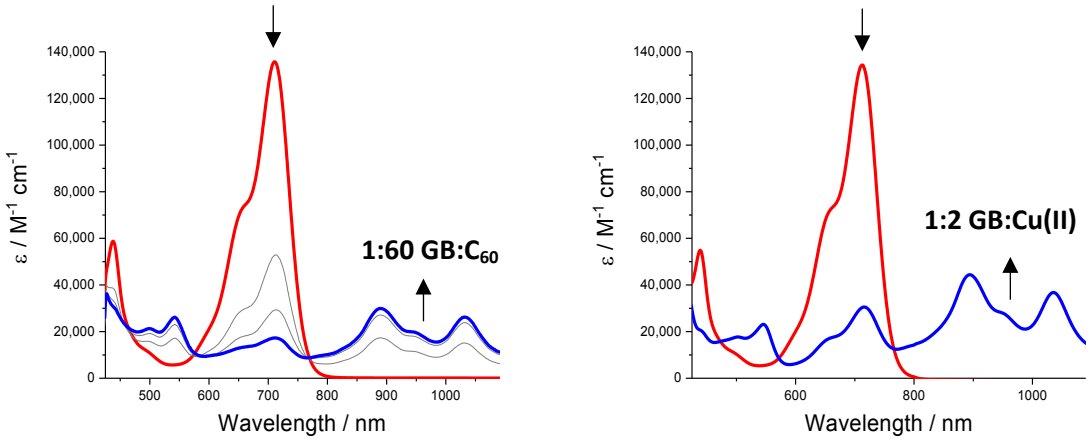


Figure S4.10. Vis-NIR absorption spectra of Green Box upon the titration with up to 60 equiv. of C_{60} (corrected for C_{60} absorptions) and a 1:2 stoichiometric mixture of Green Box **4**:Cu(II) triflate in nitrobenzene. Comparison indicates partial oxidation of the second PDI panel of Green Box can occur in the presence of a large excess of guest (i.e. for C_{60} ε = 29,800 vs 43,000 M^{-1} cm^{-1} for Cu(II) at λ_{abs} = 890 nm). However, there is only weak association with the second fullerene guest i.e. fitting of titration data to a 1:2 host:guest model indicates K_{a2} << K_{a1}.

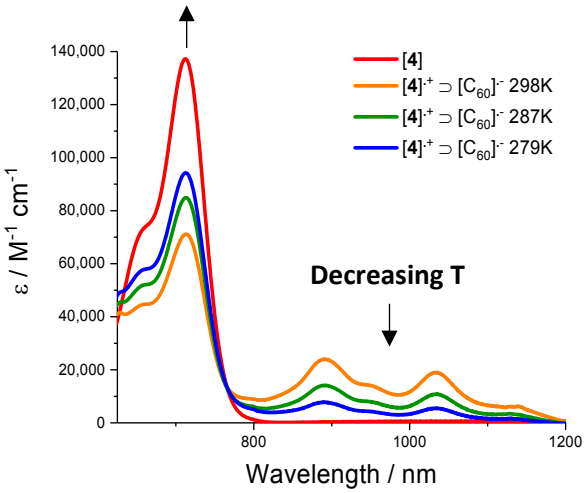


Figure S4.11. Variable temperature Vis-NIR electronic absorption spectra of the 1:1 host–guest stoichiometric complex $[\mathbf{4}]^{\cdot+}\supset[C_{60}]^{\cdot-}$ in nitrobenzene. Cooling the solution increases the yield of the neutral complex $[\mathbf{4}]^{\delta+}\supset[C_{60}]^{\delta-}$ at the expense of $[\mathbf{4}]^{\cdot+}\supset[C_{60}]^{\cdot-}$, illustrating the thermodynamic equilibrium (isosbestic point λ = 764 nm). The freezing point of nitrobenzene is 278K.

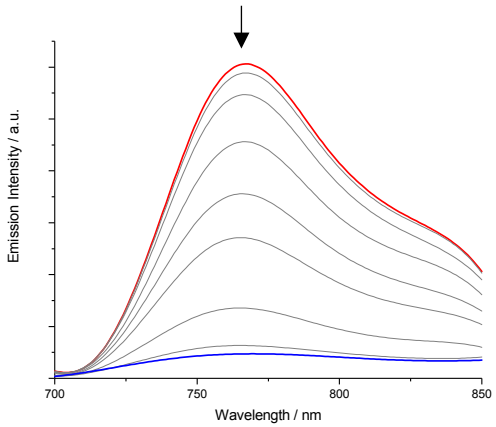


Figure S4.12. Fluorescence emission spectra of Green Box **4** upon the titration of 10 equiv. of C_{60} in nitrobenzene.

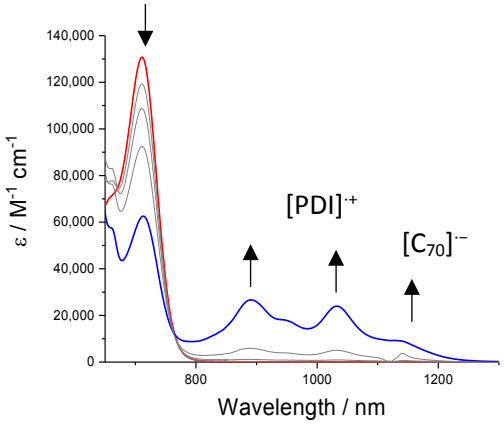


Figure S4.13. Uncorrected Vis-NIR absorption spectra of Green Box **4** upon the titration of 1.5 equiv. of C_{70} in nitrobenzene ($[C_{70}]^{\cdot-}$ λ_{abs} ~ 1150 nm).

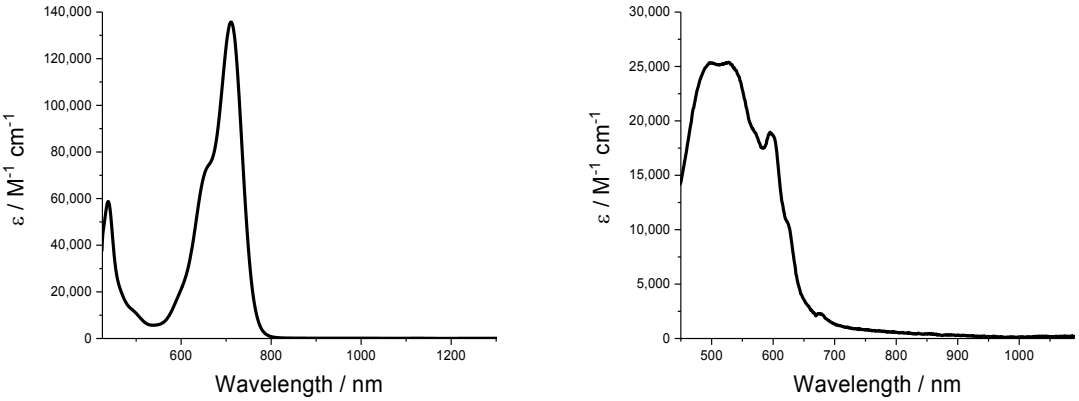


Figure S4.14. Vis-NIR absorption spectra of Green Box **4** (left) and C_{60} fullerene (right, $[C_{60}] = 10^{-4}$ M) in nitrobenzene indicating the absence of any radical ions prior to their mixing.

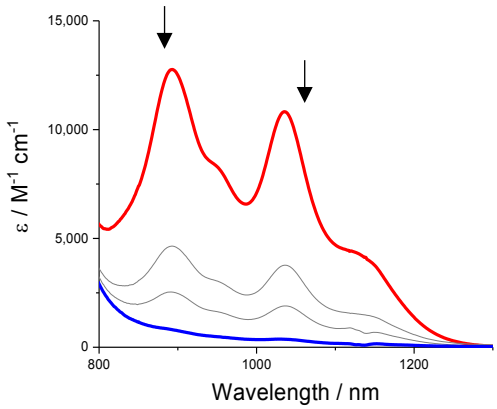


Figure S4.15. Vis-NIR absorption spectra of the 1:1 host–guest stoichiometric charge separated complex $[\mathbf{4}]^{\cdot+}\supset[C_{60}]^{\cdot-}$ (5 x 10^{-4} M) in nitrobenzene recorded over three days showing gradual reduction in concentration of radical ions.

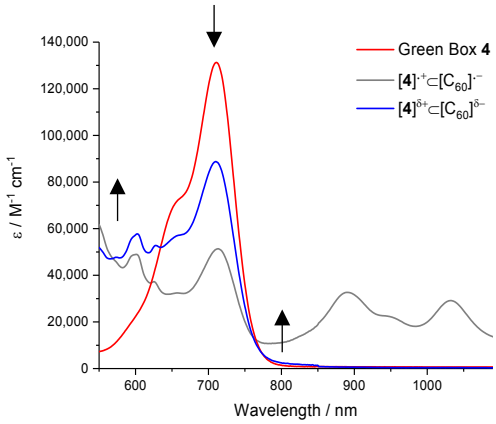


Figure S4.16. Vis-NIR absorption spectra of the 1:1 host–guest stoichiometric complex of Green Box **4** and C_{60} fullerene in nitrobenzene after three days indicating residual ground state charge transfer interactions and so the presence of the polarised complex $[\mathbf{4}]^{\delta+}\supset[C_{60}]^{\delta-}$.

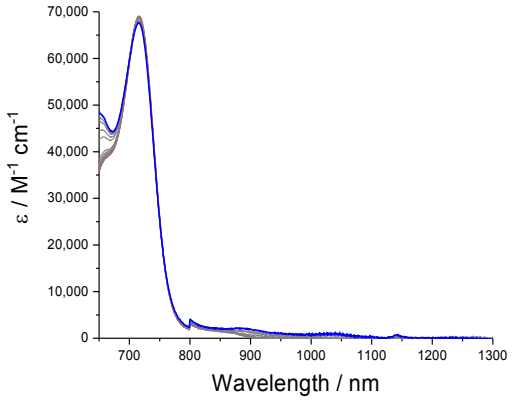


Figure S4.17. Vis-NIR absorption spectra of bis-pyrrolidine PDI single panel **5** upon the titration of 60 equiv. of C_{60} in nitrobenzene. Spectral changes, including the formation of radical ions are negligible in comparison to Green Box **4**.

b) Further comments and discussion

As expected for a [1+1] macrocycle, the extinction co-efficient of $\lambda_{abs,max}$ (ε = 136,000 M^{-1} cm^{-1}) of **4** (Figure S4.9) is a near summation of two single PDI panels, **5** (ε = 69,000 M^{-1} cm^{-1}, Figure S4.12).

From Figure 5c in the manuscript, comparable extinction co-efficients for the $[PDI]^{\cdot+}$ band at λ_{abs} = 890 nm with that of an electrochemically generated $[PDI]^{\cdot+}$ (ε = 17,300 M^{-1} cm^{-1} and 17,400 M^{-1} cm^{-1} respectively)[9] also indicates that only a single bis-pyrrolidine PDI panel of the Green Box is oxidised in $[\mathbf{4}]^{\cdot+}\supset[C_{60}]^{\cdot-}$.

For a number of previous imide-appended PDI–C_{60}-based dyads[10,11] weak electronic coupling has arisen from the existence of a node in the HOMO at the PDI imide nitrogen atoms and orthogonality of the donor–acceptor aromatic planes.[9,12] It would appear that this effect can be alleviated through the greater orbital flexibility afforded by intermolecular vs. intramolecular electronic communication in the dyad; as evidenced by significant spectroscopic changes observed upon formation of the non-covalent Green Box–fullerene complex $[\mathbf{4}]\supset[C_{60}]$ in a variety of solvents. Indeed, calculated ground and excited state dipole moments of a bis-pyrrolidine PDI show that charge is primarily transferred from nitrogen atoms in a direction perpendicular to the plane of the perylene core[9] thereby enabling an electronic interaction with the fullerene bound above it.

5. Electrochemistry

Cyclic voltammetric (CV) studies were carried out using an Autolab PGSTAT302N potentiostat, in a three-electrode arrangement in a single compartment cell. A glassy carbon working electrode, a Pt wire secondary electrode and a saturated Ag/AgCl reference electrode (chemically isolated from the test solution *via* a bridge tube containing electrolyte solution and fitted with a porous Vycor frit) were used in the cell. Experiments were performed under an atmosphere of argon and in anhydrous solvents. Sample solutions were prepared under an atmosphere of argon using Schlenk line techniques and consisted of a 0.1 M solution of the supporting electrolyte [$^{n}Bu_4N$][BF_4] and a 0.5-1 mM solution of the test compound. Redox potentials were referenced vs. the Fc^{+}/Fc couple either directly by adding an equal amount of ferrocene to the test solution. Compensation for internal resistance was not applied. Only one oxidation process was observed for **4** in o-DCB, most likely due to the low stabilisation of the oxidised states by the relatively low polarity solvent in comparison to nitrobenzene.

Table S5.1. Electrochemical data of the bis-PDI macrocycle Green Box **4** and C_{60} recorded in nitrobenzene and o-DCB in the presence of 0.1 M [$^{n}Bu_4N$][BF_4]. All electrochemical potentials quoted *vs.* Fc^{+}/Fc redox couple.

	Nitrobenzene			o-DCB	
	$E^{1/2}_{ox1}$, V	$E^{1/2}_{ox2}$, V	$E^{1/2}_{red}$, V	$E^{1/2}_{ox1}$, V	$E^{1/2}_{red}$, V
PDI single panel **5**	+0.22	+0.35	-	-	-
Green Box **4**	+0.19	+0.33	-	+0.21	-
C_{60}	-	-	−0.92	-	−1.04[13]
4+C_{60} (1:2)	+0.19	+0.32	−0.92	-	-
4+C_{60} (1:10)	+0.19	+0.33	-	+0.23	-

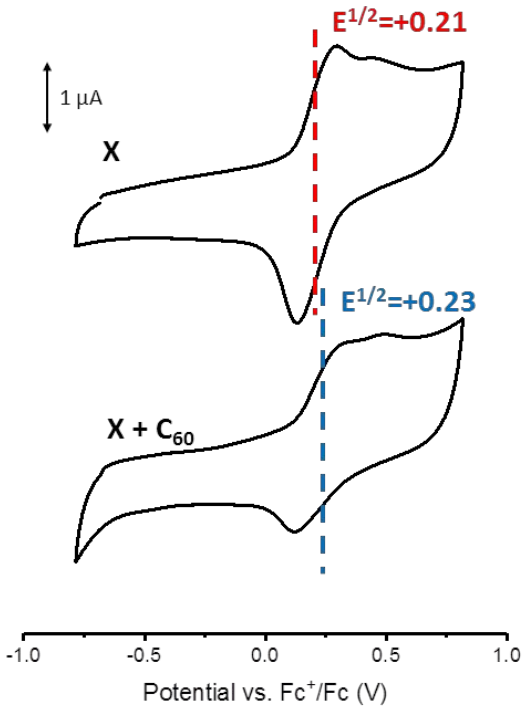


Figure S5.1. Cyclic voltammograms recorded in o-DCB of Green Box **4** (top) and $[\mathbf{4}]^{\delta+}\supset[C_{60}]^{\delta-}$ (bottom). Dashed lines indicate the position of the $E^{1/2}$ in each case.

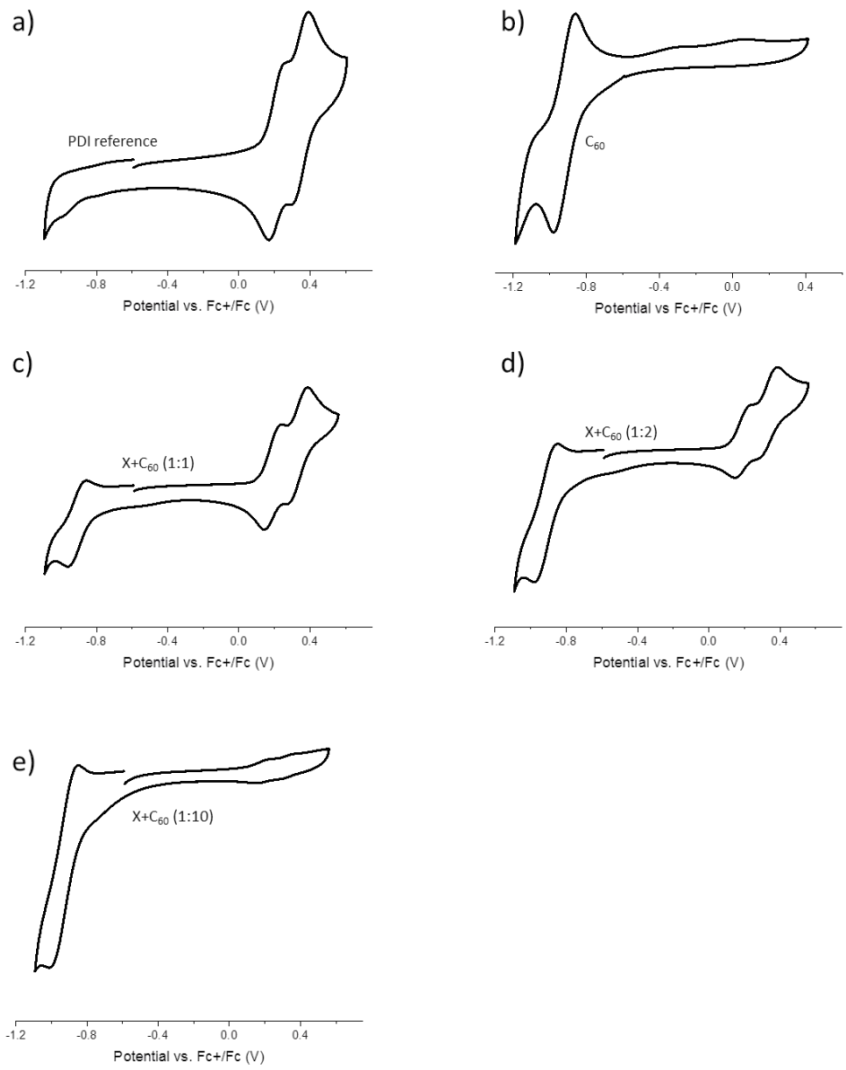


Figure S5.2. Cyclic voltammograms recorded in nitrobenzene containing 0.1M [$^{n}Bu_4N$][BF_4] at 0.1 V/s: a) bis-pyrrolidine PDI reference compound **5**; b) C_{60} fullerene; c) Green Box **4** after the addition of 1 eq. C_{60}; d) Green Box **4** after the addition of 2 eq. C_{60}; d) Green Box **4** after the addition of 10 eq. of C_{60}.

6. EPR spectroscopy

Continuous-wave electron paramagnetic resonance (CW-EPR) was acquired in the Centre for Advanced Electron Spin Resonance (CAESR) in the Department of Chemistry of the University of Oxford. X-band data collection involved use of a Bruker BioSpin EMXmicro spectrometer with a Premium-X bridge and an ER123-SHQE-W1 Bruker BioSpin resonator. The sample was placed within an Oxford Instruments ESR900 cryostat that fits within the resonator, given a resonant mode frequency of approximately 9.38 GHz. Transient EPR or time-resolved EPR (TR-EPR) made use of a Bruker BioSpin EleXSys I E680 spectrometer at both X-band and W-band (94 GHz), while the resonators were a $TE_{01\delta}$ mode cylindrical sapphire dielectric ER4118X-MD5-W1 at X-band and a cylindrical cavity TE_{011} mode EN600-1021H Teraflex ENDOR resonator at W-band. Temperature was maintained at 85 K for both frequencies with Oxford Instruments CF935 cryostats under N2 flow and an ITC-503s temperature controller. The LASER flashes of about 9 ns length for TR-EPR were produced with an Opotek Opolette HE355 LASER which features an optical parametric oscillator (OPO) crystal of beta-barium borate (BBO). For X-band the LASER beam was directed into the X-band resonator and cryostat windows via turning mirrors and at W-band it was conveyed via a fibre coupling with ThorLabs FT600UMT 0.39 NA multimode fibre of 0.6 mm O.D. core threaded into a standard insertion rod and made vacuum tight with Dow Corning silicone high vacuum grease. The LASER repetition rate was 20 Hz with a pulse energy of 1.5 mJ at X-band and 450 µJ at W-band. The master time synchronization of LASER flash lamp, Q-switch and E680 spectrometer was a Stanford Research DG645 delay generator. The triplet state and CW-EPR simulations employed the EasySpin toolbox in Matlab (MathWorks, Inc.).[14]

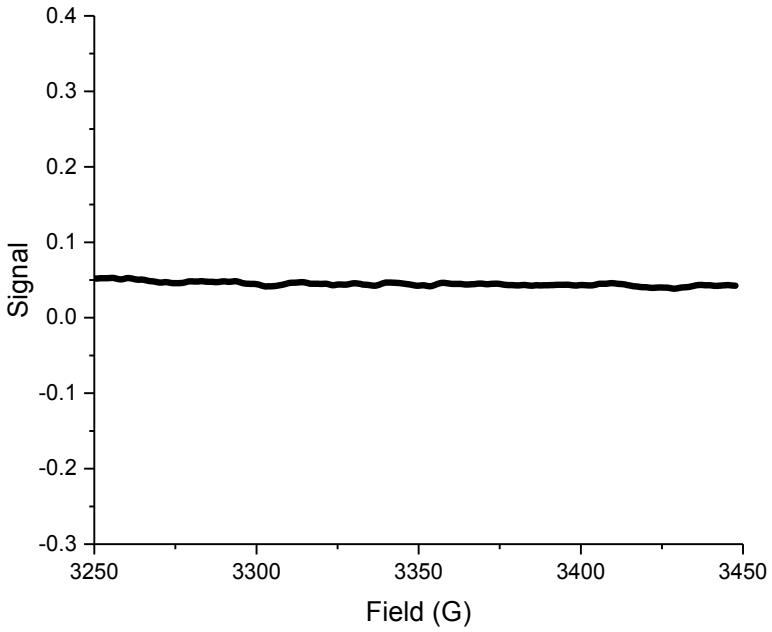


Figure S6.1. EPR spectrum of C_{60} in nitrobenzene showing the absence of any radical species (10^{-4} M).

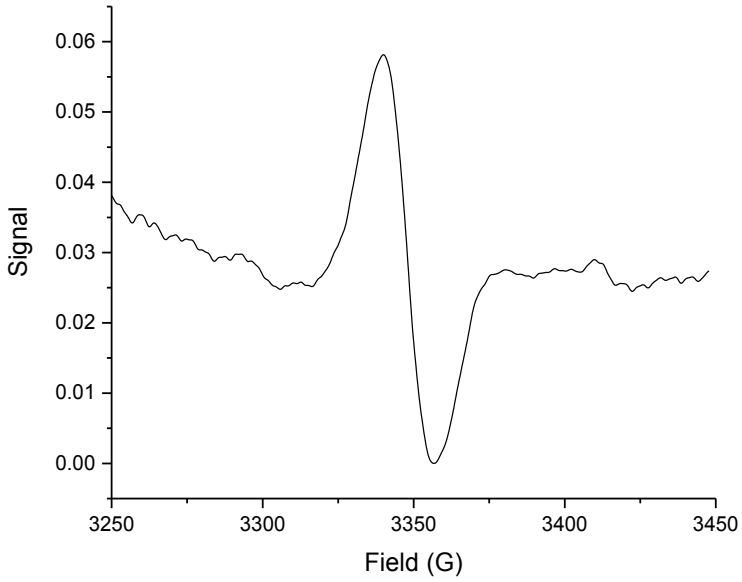


Figure S6.2. EPR spectrum of $[\mathbf{4}]^{\cdot+}\supset[C_{60}]^{\cdot-}$ after two weeks on the bench showing persistence of the radical pair in nitrobenzene.

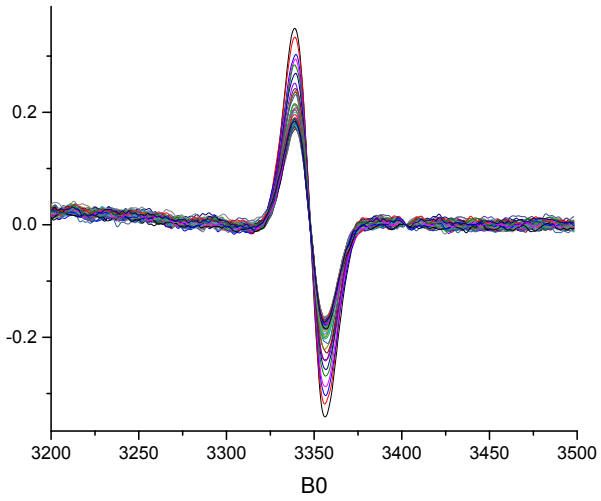


Figure S6.3. EPR spectra showing gradual decrease in intensity of signal for the radical pair over 10 hours.

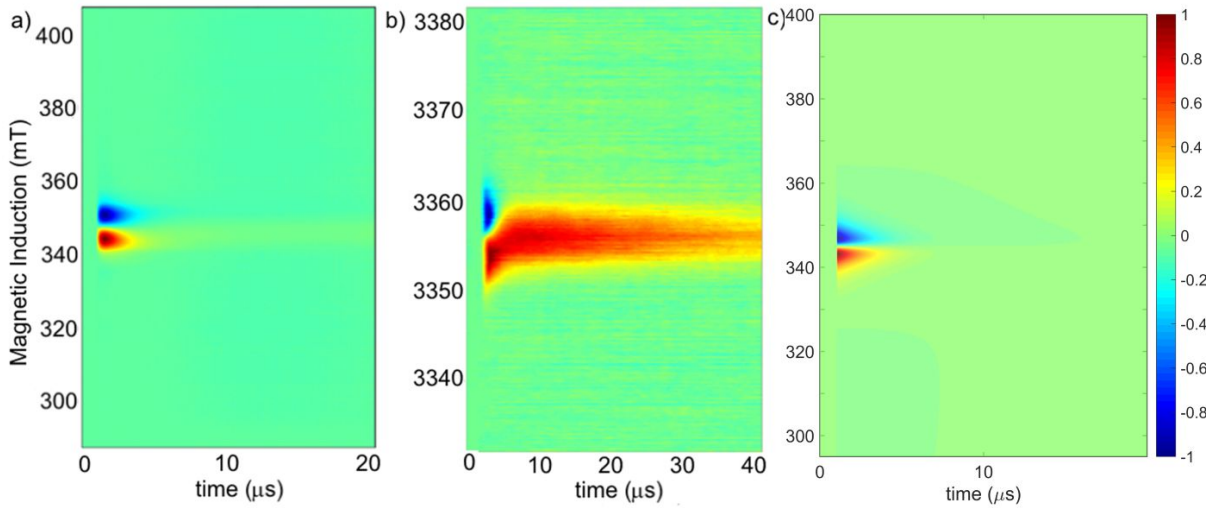


Figure S6.4. TR-EPR spectra at 85 K and 600 nm excitation of two 100 □M samples of in frozen toluene, for [**4**]⊃[C_{60}] at X-band (panel a) and W-band (panel b) and simulation of the X-band data in the isotropic limit (panel c, with acquisition trigger time offset). The colour bar on the far right has red as positive and blue as negative, representing microwave absorption and emission, respectively. The data was collected as described in the EPR Spectroscopy methods section and the simulation was a spin dynamics calculation in Matlab. The microwave frequencies were 9.7313 and 93.956 GHz, for a) and b) respectively.

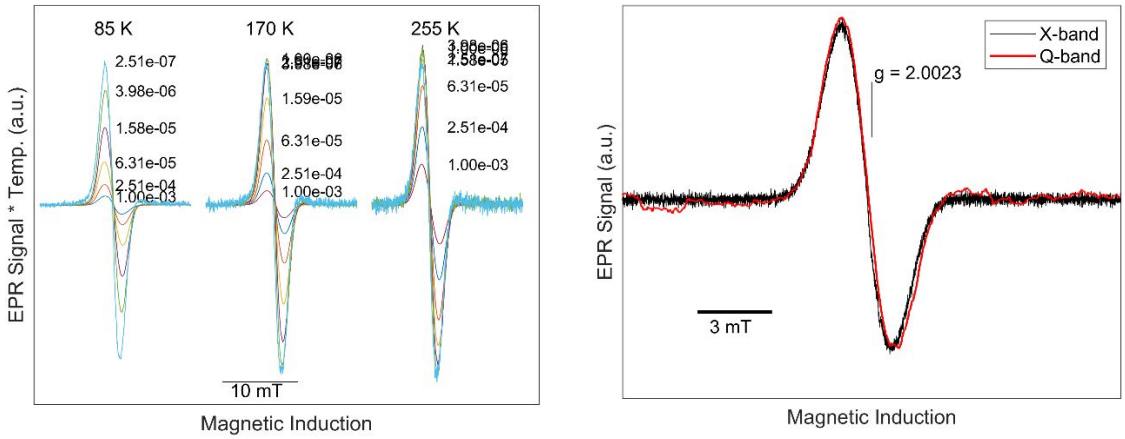


Figure S6.5. Frozen solution CW-EPR of the [**4**]⊃[C_{60}] prepared in nitrobenzene. On left, CW-EPR at 85 K, 170 K, and 255 K, with microwave power indicated in Watts and maxima. The microwave frequencies were 9.689 GHz, 9.723 GHz and 9.632 GHz with respect to temperature. The modulation amplitude was 0.5 mT. On right, CW-EPR of the frozen solution at two frequencies with acquisition parameter values: temperature 255 K frequency of 9.6297 GHz, microwave power 3.9830×10^{-6} W, modulation amplitude of 0.5 G and 57 sweeps of 671.09 sec., microwave power 5.024×10^{-6} W, and temperature 85 K, frequency of 34.0174 GHz, 1.5 G, 89 sweeps of 600 sec., for X-band and Q-band, respectively.

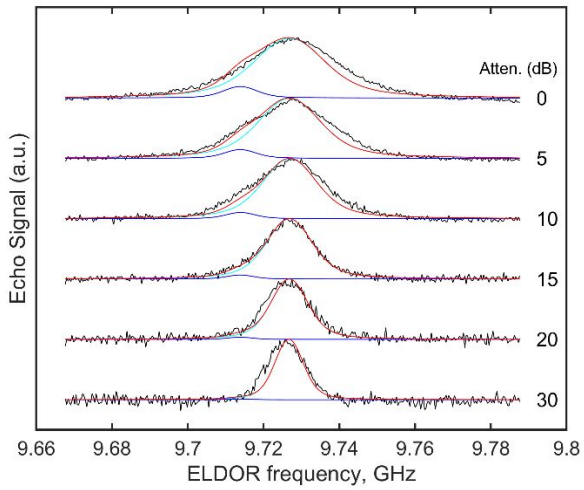


Figure S6.6. ELDOR pulsed EPR of photo-excited [**4**]⊃[C_{60}] prepared in toluene. An inversion pulse of 32 ns was followed by a 500 ns ELDOR pulse with sufficient time (2 μs) for decoherence prior to 16-32ns echo detection following the literature reference.[15] A representative plot of two Gaussian lines that broaden with ELDOR power are in blue (-12 MHz) and cyan with the summation in red.

7. Kinetic data

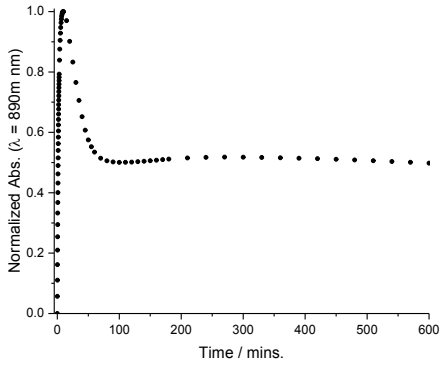


Figure S7.1. Time course measurement of $[\mathbf{4}]^{\cdot+}\supset[C_{60}]^{\cdot-}$ (1:5 host–guest stoichiometric ratio, [**4**] = 10^{-4} M) by electronic absorption spectroscopy (λ = 890 nm) in nitrobenzene showing persistence of $[PDI]^{\cdot+}$ in solution with $t_{½}$ > 600 minutes.

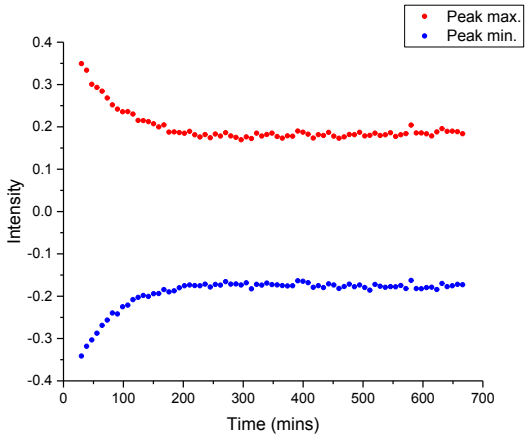


Figure S7.2. Time course measurement of $[\mathbf{4}]^{\cdot+}\supset[C_{60}]^{\cdot-}$ (1:1 host–guest stoichiometric ratio, [**4**] = 10^{-4} M) by EPR spectroscopy (maxima and minima of peak) in nitrobenzene showing persistence of $[C_{60}]^{\cdot-}$ in solution. NB. There was a 30 minute delay between sample preparation and measurement of the first EPR spectrum, preventing accurate calculation of $t_{½}$.

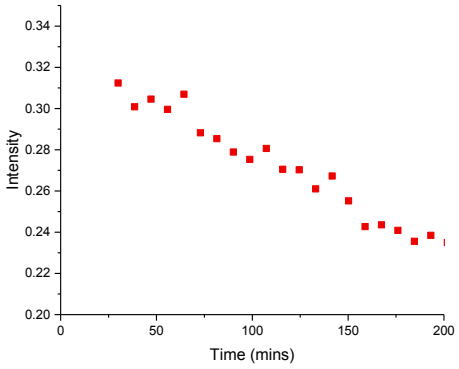


Figure S7.3. Time course measurement over first 200 minutes of $[\mathbf{4}]^{\cdot+}\subset[C_{60}]^{\cdot-}$ by EPR spectroscopy in nitrobenzene *under dinitrogen* showing similar behaviour to oxygenated conditions (1:1 host–guest stoichiometric ratio, [**4**] = 10^{-4} M).

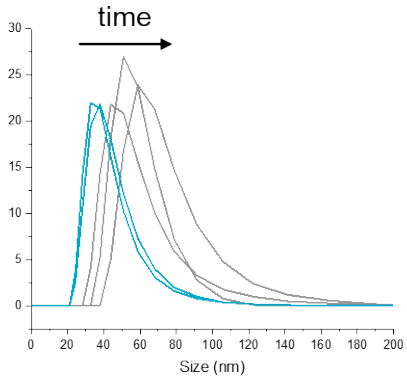


Figure S7.4. Dynamic light scattering intensity distribution of [**4**]⊂[C_{60}] in nitrobenzene over two hours showing the average particle size is over doubled. This is due to C_{60} because analysis of C_{60} alone revealed similar behaviour.

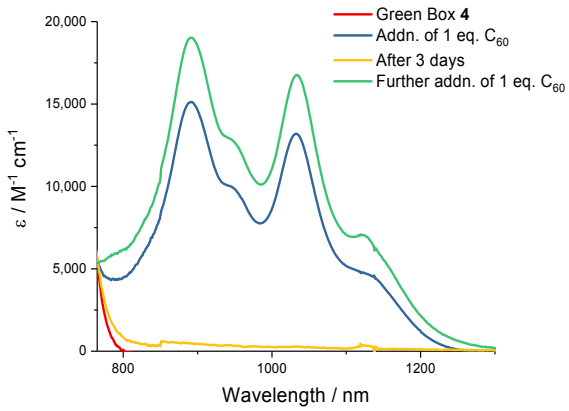


Figure S7.5. Vis-NIR absorption spectra showing regeneration of radical ions $[\mathbf{4}]^{\cdot+}\subset[C_{60}]^{\cdot-}$ in nitrobenzene, after their depletion, through the addition of a further equivalent of C_{60} fullerene.

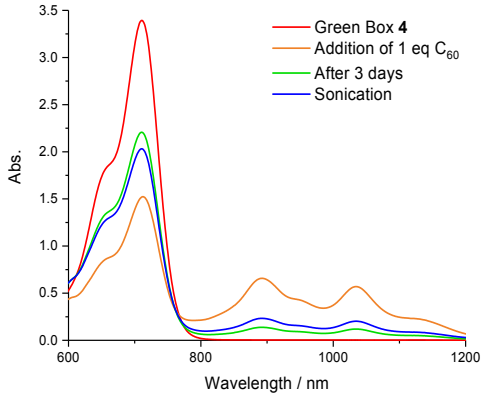


Figure S7.6. Vis-NIR absorption spectra showing regeneration of radical ions $[\mathbf{4}]^{\cdot+}\subset[C_{60}]^{\cdot-}$ in nitrobenzene, after their depletion, through five minutes sonication.

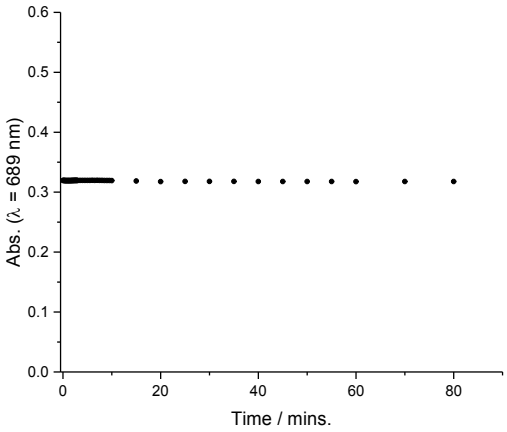
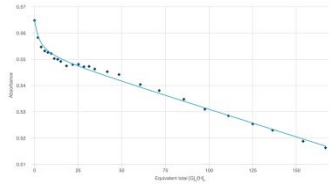


Figure S7.7. Time course measurement of $[\mathbf{4}]^{\delta+}\supset[C_{60}]^{\delta-}$ by electronic absorption spectroscopy (λ = 689 nm) in toluene showing no time dependence to the spectral changes arising from partial charge transfer interactions ([**4**] = 10^{-5} M).

8. Bindfit data

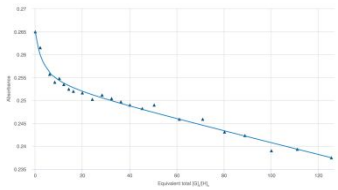
Vis-NIR spectroscopic titration curves for Green Box **4** upon the titration with up to 170 eq. of C_{60} or C_{70} fullerene guest. Association constants obtained from binding curves through multiwavelength fitting of the largest spectral changes, which occurred to the main PDI absorption band (λ = 690 – 720 nm). This region was also chosen because the absence of spectral overlap with fullerene bands permitted the use of non-corrected absorption spectra thus minimizing error. The Job's plot analysis is considered appropriate when there is a 1:1 host–guest stoichiometric complex,[16] and so has been performed for C_{60} binding in nitrobenzene. However, when more than one complex is present, i.e. 1:2 host–guest binding, the Job's method is considered unreliable such that non-sigmoidal residues and low fitting covariances are better indicators of an appropriate binding model.[17–19] All fitting errors < 10 %. Solid points represent experimental data; continuous line represents theoretical binding isotherm. Average values from three experiments have been taken. Relative standard deviations are provided, and all are < 8%. For toluene and o-DCB, since K_{a1} >> K_{a2}, the fitting to a 1:1 host–guest binding model at early stage of titration is shown where possible. Stronger binding in nitrobenzene made a 1:1 host–guest model a superior fit than a 1:2 model. As such, a Jobs Plot was performed for this data set.

a) Green Box + C_{60} in toluene



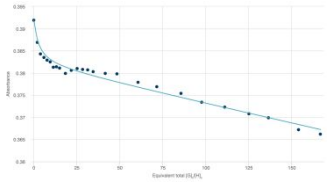
K_{a1} = 42,150

K_{a2} < 1



K_{a1} = 40,001

K_{a2} < 1



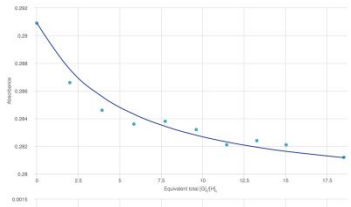
K_{a1} = 42,007

K_{a2} < 1

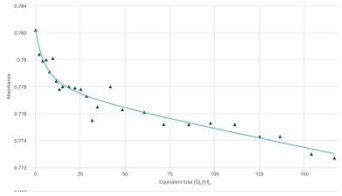
Mean (K_{a1}) = 41,389

Rel. st. dev. (K_{a1}) = 2.37%

1:1 host:guest model fitting of first 10 titration points:

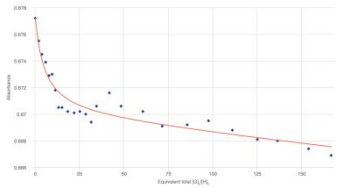


b) Green Box + C_{70} in toluene



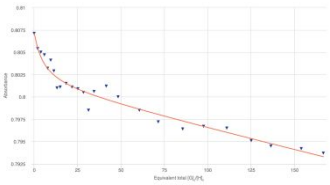
K_{a1} = 20,503

K_{a2} < 1



K_{a1} = 21,024

K_{a2} < 1



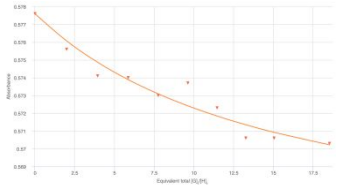
K_{a1} = 19,616

K_{a2} < 1

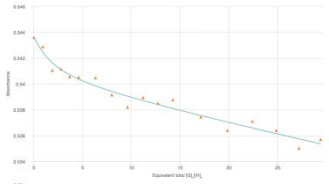
Mean (K_{a1}) = 20,381

Rel. st. dev. (K_{a1}) = 2.85%

1:1 host:guest model fitting of first 10 titration points:

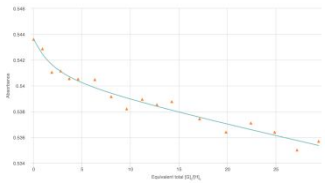


c) Green Box + C_{60} in o-DCB



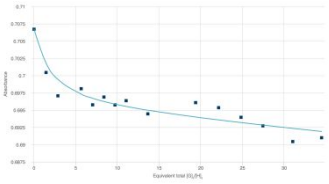
K_{a1} = 68,538

K_{a2} = 83



K_{a1} = 70,288

K_{a2} = 108



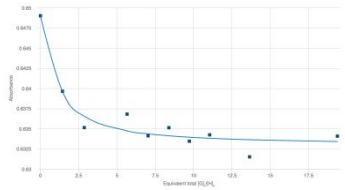
K_{a1} = 70,855

K_{a2} = 98

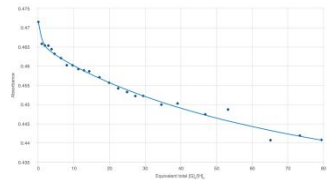
Mean (K_{a1}) = 69,894

Rel. st. dev. (K_{a1}) = 1.41%

1:1 host:guest model fitting of first 10 titration points:

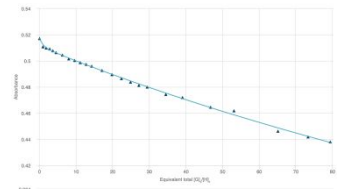


d) Green Box + C_{70} in o-DCB



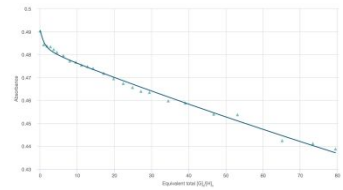
K_{a1} = 72,499

K_{a2} = 102



K_{a1} = 70,999

K_{a2} = 101



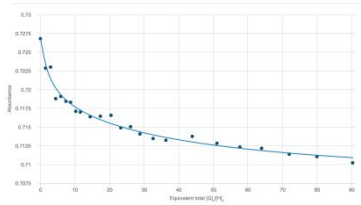
K_{a1} = 71,500

K_{a2} = 102

Mean (K_{a1}) = 71,667

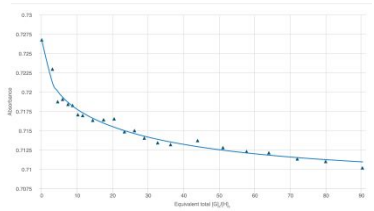
Rel. st. dev. (K_{a1}) = 0.87%

d) Green Box + C_{60} in 1:1 nitrobenzene:toluene



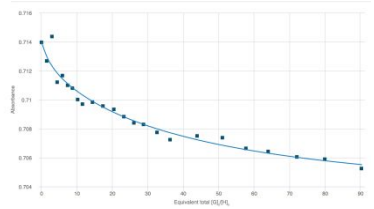
K_{a1} = 53,420

K_{a2} < 10



K_{a1} = 54,381

K_{a2} < 10



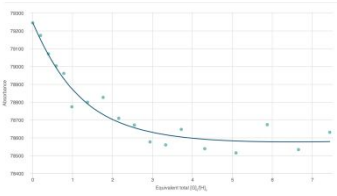
K_{a} = 51,603

K_{a2} < 10

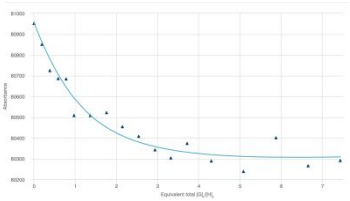
Mean (K_{a1}) = 53,134

Rel. st. dev. (K_{a1}) = 2.17 %

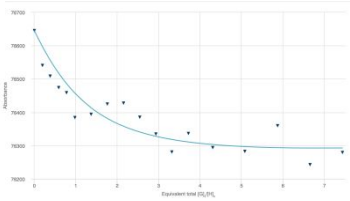
e) Green Box + C_{60} in nitrobenzene



K_a = 142,510



K_a = 149,387



K_a = 123,342

Mean (K_a) = 138,413

Rel. st. dev. (K_a) = 7.96 %

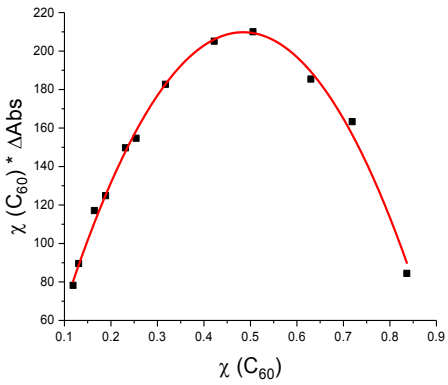


Figure S8.1. Job's plot analysis for C binding to Green Box **4** in nitrobenzene indicates a 1:1 host–guest binding stoichiometry; the maximum change in absorbance occurs when the mole fraction of fullerene guest χ (C_{60}) = 0.5.

9. Free energy of photoinduced electron transfer

The free energy for photoinduced electron transfer and charge separation (CS) in eV from the PDI donor (D) excited singlet state to C_{60} acceptor (A) in complex [**4**]⊃[C_{60}] can be estimated by:[20]

$-\Delta G_{CS} = \Delta E_{0\text{-}0} + \Delta G_{CR}$

Where $\Delta E_{0\text{-}0}$ is the energy level of the lowest singlet excited state of the PDI as determined from the intersection of the absorption and fluorescence emission spectra and ΔG_{CR} is the driving force for charge recombination (CR) in eV calculated by:

$-\Delta G_{CR} = e[E_{ox}(D/D^{+}) - - E_{red}(A/A^{-})] + \Delta G_{s}$

The correction term (ΔG_s) for the effects of solvent polarity is often found to be negligible in solvents of moderate polarity such as o-DCB (ε = 9.9). Therefore, using the electrochemical data recorded in o-DCB (Table S5.1) and without the correction term, for complex [**4**]⊃[C_{60}]; $-\Delta G_{CR}$ = 1.25 eV.

Since for [**4**]⊃[C_{60}] $\Delta E_{0\text{-}0}$ = 1.74 eV ; $-\Delta G_{CS}$ = 0.49 eV indicated that excited state electron transfer processes were energetically favourable in the complex.

This value is in good agreement with that from a previously reported covalently linked bis-pyrrolidine–C_{60} dyad.[20,21]

10. Molecular Modeling

Methods

4 was generated through atomic manipulation of single crystal X-ray diffraction structures, deposited with the Cambridge Crystallographic Data Centre (CCDC).[22] The PDI panels were obtained from the crystal structure with the CSD RefCode YOYTUB,[23] while the biphenyl-triazole moieties were taken from the crystal structure with the CSD RefCode EWEQIH.[24] C_{60} was obtained from the crystal structure with the CSD RefCode AGIGEF.[25]

A preliminary conformational search for [**4**]⊃[C_{60}] binding arrangements in gas-phase was carried using AMBER18.[26] Both the host and the guest were described with the General AMBER Force Field,[27,28] along with MOPAC charges obtained after optimizing each components in PM7 with MOPAC2016.[29] The initial host-guest complex [**4**]⊃[C_{60}]was subjected to a gas-phase conformational analysis process, consisting of an initial molecular mechanics (MM) energy minimization, followed by a heating stage to 300 K for 50 ps, and ensued by a collection run of 500 ps, using a time step of 1 fs. 5000 structures resulted from this run, which were saved and further energy minimized by MM until the convergence criterion of 0.0001 kcal mol^{-1} was achieved. This process was undertaken in 5 independent runs, yielding 25000 structures. Binding arrangements ***A*** and ***B*** were selected from a RMSD clustering analysis of these data.

As a technical note, given the size of the Green Box-C_{60} fullerene complex, it was only possible to carry out partial frequency calculations in gas-phase for the host, with the guest frozen. Still, in these conditions, no imaginary frequencies were found. Naturally, other conformational binding scenarios beyond ***A*** and ***B*** with different energies are possible (*vide supra*). These putative structures would be mainly derived through the variations of the endocyclic torsion angles on the flexible alkyl spacers, as observed in the preliminary conformational analysis carried out for Green Box-C_{60} host-guest complex.

The Natural Population Analysis charges were determined *via* Natural Bond Orbital analysis,[30] through the NBO 3.1 executable[31] as implemented in Gaussian09.[32]

Additional figures, schemes, and tables

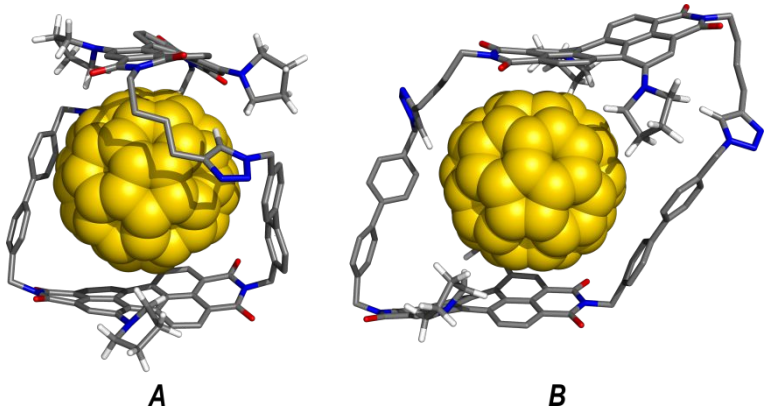


Figure S10.1. DFT structures of [**4**]⊃[C_{60}] of binding arrangements ***A*** and ***B*** optimised in nitrobenzene for the singlet state. The C_{60} guest is shown in spheres and the macrocyclic host is shown in sticks, with the C-H protons hidden for clarity, except those in the triazole and pyrrolidine moieties.

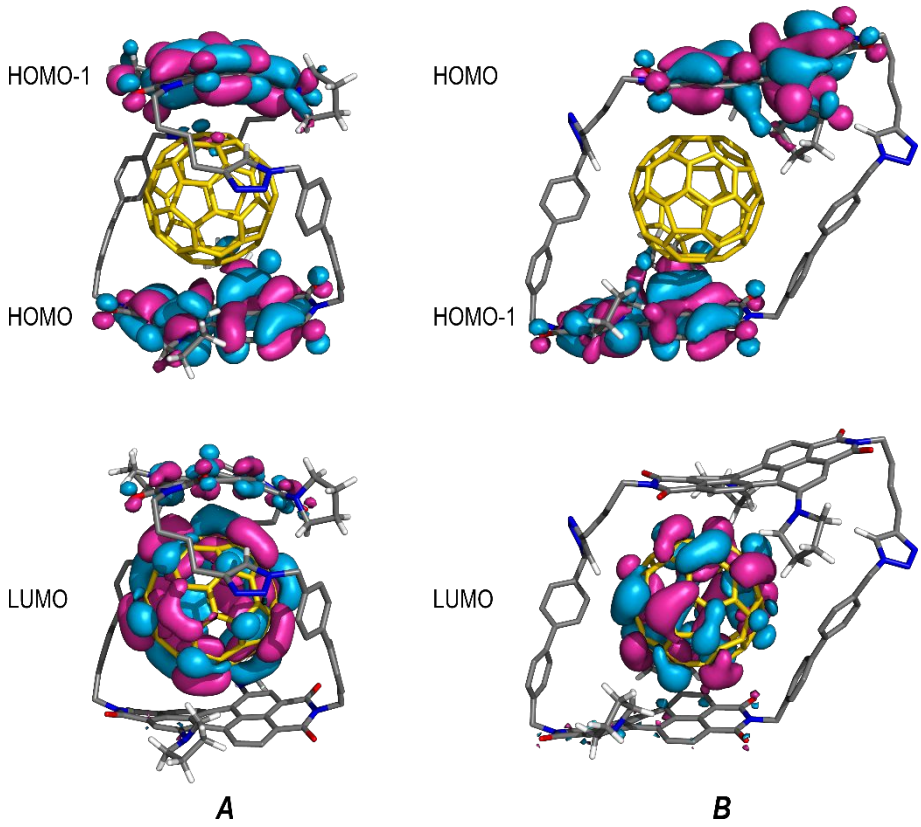


Figure S10.2. Isodensity surface plots of frontier molecular orbitals HOMO-1, HOMO and LUMO of [**4**]⊃[C_{60}] in binding arrangements ***A*** and ***B***, for the singlet state optimized structures in toluene (density value of ±0.015 ea_0^{-3}).

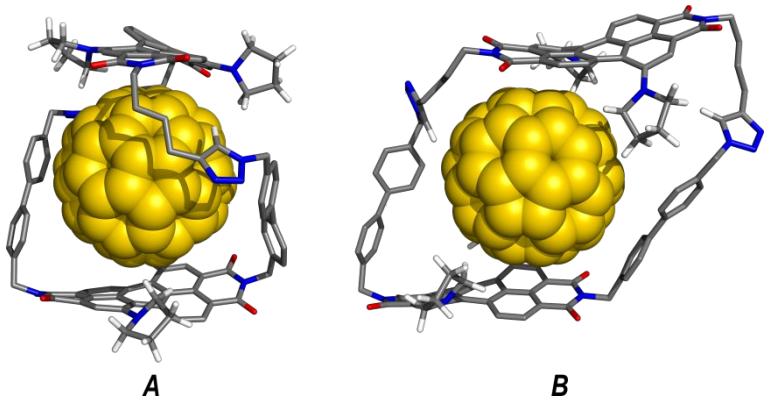
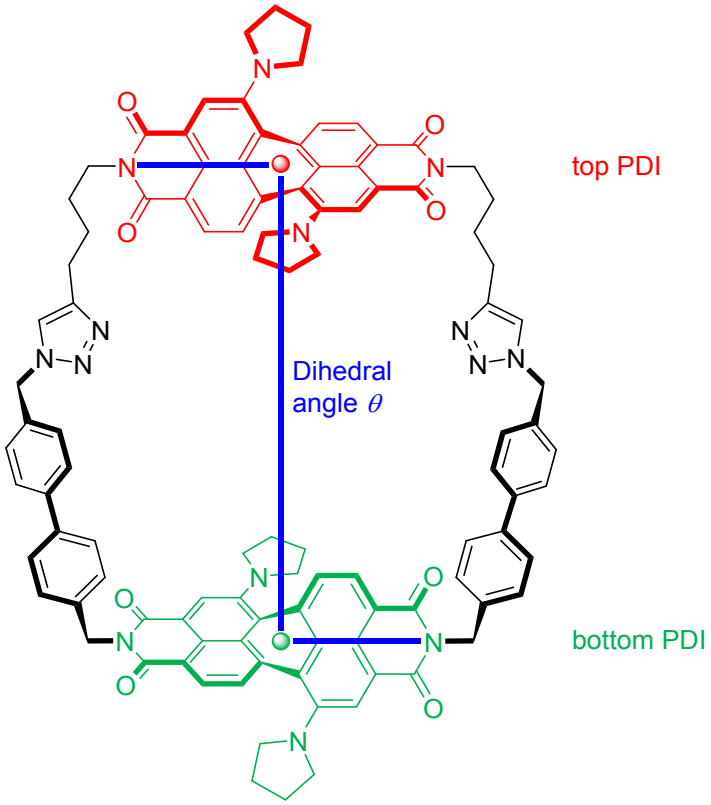


Figure S10.3. DFT structures of [**4**]⊃[C_{60}] of binding arrangements ***A*** and ***B*** optimised in nitrobenzene for the triplet state. The C_{60} guest is shown in spheres and the macrocyclic host is shown in sticks, with the C-H protons hidden for clarity, except those in the triazole and pyrrolidine moieties.



Scheme S10.1.

Table S10.1. RMSD (Å) between DFT optimized structures of singlet state [**4**]⊃[C_{60}] in gas-phase, toluene and nitrobenzene.

	Binding arrangement			
	A		***B***	
	Toluene	Nitrobenzene	Toluene	Nitrobenzene
Gas	0.42	0.42	0.28	0.40
Toluene	–	0.07	–	0.27

Table S10.2. Structural parameters assessed in the DFT optimized structures of [**4**]⊃[C_{60}].

Binding arrangement	***A***	***B***	***A***	***B***	***A***	***B***	***A***	***B***
State			Singlet				Triplet	
Medium	Gas		Toluene		Nitrobenzene			
Dihedral angle θ (°)	62.8; 66.6	21.5; 18.9	71.3; 69.5	22.2; 20.4	71.4; 69.6	26.1; 24.2	69.5; 74.0	26.6; 24.5
Distances (Å)[a]								
PDI depth	0.58; *0.41*	-0.71; *-0.34*	0.40; *0.32*	-0.69; *-0.32*	0.41; *0.32*	-0.66; *-0.38*	0.35; *0.26*	-0.70; *-0.37*
C_{60}···PDI_{C6}	3.37; *3.48*	–	3.43; *3.60*	–	3.44; *3.59*	–	3.32; *3.62*	–
C_{60}···PDI_{half}	–	3.40; *3.30*	–	3.40; *3.34*	–	3.44; *3.37*	–	3.45; *3.38*
C-H_{pyr}···C_{60}	2.69; 3.59; *2.62*; *2.62*	2.87; 2.93; *2.62*; *2.82*	2.58; 3.36; *2.56*; *2.66*	2.83; 3.03; *2.67*; *2.77*	2.61; 3.36; *2.56*; *2.67*	2.91; 2.97; *2.67*; *2.75*	2.63; 3.67; *2.56*; *2.64*	2.85; 2.97; *2.64*; *2.74*

[a] The values given in italics are for the bottom PDI.

Table S10.3. HOMO-1, HOMO and LUMO energies (in eV), for the toluene and nitrobenzene DFT optimized structures of [**4**]⊃[C_{60}] in binding arrangements ***A*** and ***B***

Implicit solvent	Binding arrangement	HOMO-1	HOMO	LUMO
Toluene	***A***	-7.15	-6.85	-1.81
	B	-6.62	-6.54	-1.88
Nitrobenzene	***A***	-6.94	-6.75	-1.62
	B	-6.44	-6.36	-1.62

Tables S10.4, S10.5 and **S10.6** are available to download.

11. References

(1) Lee, B.-Y.; Park, S. R.; Jeon, H. B.; Kim, K. S. A New Solvent System for Efficient Synthesis of 1,2,3-Triazoles. *Tetrahedron Letters* **2006**, *47* (29), 5105–5109. https://doi.org/10.1016/j.tetlet.2006.05.079.

(2) Beauvilliers, E. E.; Topka, M. R.; Dinolfo, P. H. Synthesis and Characterization of Perylene Diimide Based Molecular Multilayers Using CuAAC: Towards Panchromatic Assemblies. *RSC Adv.* **2014**, *4* (62), 32866–32875. https://doi.org/10.1039/C4RA04512B.

(3) Würthner, F.; Stepanenko, V.; Chen, Z.; Saha-Möller, C. R.; Kocher, N.; Stalke, D. Preparation and Characterization of Regioisomerically Pure 1,7-Disubstituted Perylene Bisimide Dyes. *J. Org. Chem.* **2004**, *69* (23), 7933–7939. https://doi.org/10.1021/jo048880d.

(4) Shibano, Y.; Umeyama, T.; Matano, Y.; Imahori, H. Electron-Donating Perylene Tetracarboxylic Acids for Dye-Sensitized Solar Cells. *Org. Lett.* **2007**, *9* (10), 1971–1974. https://doi.org/10.1021/ol070556s.

(5) Saito, Y.; Matsumoto, K.; Bag, S. S.; Ogasawara, S.; Fujimoto, K.; Hanawa, K.; Saito, I. C8-Alkynyl- and Alkylamino Substituted 2′-Deoxyguanosines: A Universal Linker for Nucleic Acids Modification. *Tetrahedron* **2008**, *64* (16), 3578–3588. https://doi.org/10.1016/j.tet.2008.01.091.

(6) Hancock, L. M.; Beer, P. D. Sodium and Barium Cation-Templated Synthesis and Cation-Induced Molecular Pirouetting of a Pyridine N-Oxide Containing [2]Rotaxane. *Chem. Commun.* **2011**, *47* (21), 6012–6014. https://doi.org/10.1039/C1CC11224D.

(7) Chao, C.-C.; Leung, M.; Su, Y. O.; Chiu, K.-Y.; Lin, T.-H.; Shieh, S.-J.; Lin, S.-C. Photophysical and Electrochemical Properties of 1,7-Diaryl-Substituted Perylene Diimides. *J. Org. Chem.* **2005**, *70* (11), 4323–4331. https://doi.org/10.1021/jo050001f.

(8) Stinchcombe, J.; Penicaud, A.; Bhyrappa, P.; Boyd, P. D. W.; Reed, C. A. Buckminsterfulleride(1-) Salts: Synthesis, EPR, and the Jahn-Teller Distortion of C60-. *J. Am. Chem. Soc.* **1993**, *115* (12), 5212–5217. https://doi.org/10.1021/ja00065a037.

(9) Lukas, A. S.; Zhao, Y.; Miller, S. E.; Wasielewski, M. R. Biomimetic Electron Transfer Using Low Energy Excited States: A Green Perylene-Based Analogue of Chlorophyll a. *J. Phys. Chem. B* **2002**, *106* (6), 1299–1306. https://doi.org/10.1021/jp014073w.

(10) Baffreau, J.; Leroy-Lhez, S.; Vân Anh, N.; Williams, R. M.; Hudhomme, P. Fullerene C60–Perylene-3,4:9,10-Bis(Dicarboximide) Light-Harvesting Dyads: Spacer-Length and Bay-Substituent Effects on Intramolecular Singlet and Triplet Energy Transfer. *Chem. Eur. J.* **2008**, *14* (16), 4974–4992. https://doi.org/10.1002/chem.200800156.

(11) Hua, J.; Meng, F.; Ding, F.; Li, F.; Tian, H. Novel Soluble and Thermally-Stable Fullerene Dyad Containing Perylene. *J. Mater. Chem.* **2004**, *14* (12), 1849–1853. https://doi.org/10.1039/B316996K.

(12) Langhals, H.; Demmig, S.; Huber, H. Rotational Barriers in Perylene Fluorescent Dyes. *Spectrochimica Acta Part A: Molecular Spectroscopy* **1988**, *44* (11), 1189–1193. https://doi.org/10.1016/0584-8539(88)80091-6.

(13) Mancel, D.; Jevric, M.; Davies, E. S.; Schröder, M.; Khlobystov, A. N. Triad and Cyclic Diad Compounds of [60]Fullerene with Metallocenes. *Dalton Trans.* **2013**, *42* (14), 5056–5067. https://doi.org/10.1039/C3DT32626H.

(14) Stoll, S.; Schweiger, A. EasySpin, a Comprehensive Software Package for Spectral Simulation and Analysis in EPR. *Journal of Magnetic Resonance* **2006**, *178* (1), 42–55. https://doi.org/10.1016/j.jmr.2005.08.013.

(15) Maeda, K.; Storey, J. G.; Liddell, P. A.; Gust, D.; Hore, P. J.; Wedge, C. J.; Timmel, C. R. Probing a Chemical Compass: Novel Variants of Low-Frequency Reaction Yield Detected Magnetic Resonance. *Phys. Chem. Chem. Phys.* **2015**, *17* (5), 3550–3559. https://doi.org/10.1039/C4CP04095C.

(16) Atwood, J. L. et al., Comprehensive Supramolecular Chemistry II; Elsevier, 2017, ISBN: 9780128031988

(17) Hibbert, D. B.; Thordarson, P. The Death of the Job Plot, Transparency, Open Science and Online Tools, Uncertainty Estimation Methods and Other Developments in Supramolecular Chemistry Data Analysis. *Chem. Commun.* **2016**, *52* (87), 12792–12805. https://doi.org/10.1039/C6CC03888C.
(18) Thordarson, P. Determining Association Constants from Titration Experiments in Supramolecular Chemistry. *Chem. Soc. Rev.* **2011**, *40* (3), 1305–1323. https://doi.org/10.1039/C0CS00062K.
(19) Schneider, H-J.; Yatsimirsky, Y., Principles and Methods in Supramolecular Chemistry; Wiley, 2000, ISBN: 978-0-471-97253-2
(20) Shibano, Y.; Umeyama, T.; Matano, Y.; Tkachenko, N. V.; Lemmetyinen, H.; Araki, Y.; Ito, O.; Imahori, H. Large Reorganization Energy of Pyrrolidine-Substituted Perylenediimide in Electron Transfer. *J. Phys. Chem. C* **2007**, *111* (16), 6133–6142. https://doi.org/10.1021/jp068893q.
(21) Shibano, Y.; Umeyama, T.; Matano, Y.; Tkachenko, N. V.; Lemmetyinen, H.; Imahori, H. Synthesis and Photophysical Properties of Electron-Rich Perylenediimide-Fullerene Dyad. *Org. Lett.* **2006**, *8* (20), 4425–4428. https://doi.org/10.1021/ol061506a.
(22) Groom, C. R.; Bruno, I. J.; Lightfoot, M. P.; Ward, S. C. The Cambridge Structural Database. *Acta Cryst B* **2016**, *72* (2), 171–179. https://doi.org/10.1107/S2052520616003954.
(23) Langhals, H. Cyclic Carboxylic Imide Structures as Structure Elements of High Stability. Novel Developments in Perylene Dye Chemistry. *HETEROCYCLES* **1995**, *40* (1), 477. https://doi.org/10.3987/REV-94-SR2.
(24) Li, Y.; Zhao, Y.; Flood, A. H.; Liu, C.; Liu, H.; Li, Y. Nanometer-Sized Reactor—A Porphyrin-Based Model System for Anion Species. *Chemistry – A European Journal* **2011**, *17* (27), 7499–7505. https://doi.org/10.1002/chem.201100633.
(25) Lu, R.-Q.; Wu, S.; Bao, Y.-H.; Yang, L.-L.; Qu, H.; Saha, M.; Wang, X.-Y.; Zhuo, Y.-Z.; Xu, B.; Pei, J.; et al. Cocrystallization of Imide-Fused Corannulene Derivatives and C60: Guest-Induced Conformational Switching and 1:1 Segregated Packing. *Chemistry – An Asian Journal* **2018**, *13* (19), 2934–2938. https://doi.org/10.1002/asia.201801086.
(26) D.A. Case, I.Y. Ben-Shalom, S.R. Brozell, D.S. Cerutti, T.E. Cheatham, III, V.W.D. Cruzeiro, T.A. Darden, R.E. Duke, D. Ghoreishi, M.K. Gilson, H. Gohlke, A.W. Goetz, D. Greene, R Harris, N. Homeyer, S. Izadi, A. Kovalenko, T. Kurtzman, T.S. Lee, S. LeGrand, P. Li, C. Lin, J. Liu, T. Luchko, R. Luo, D.J. Mermelstein, K.M. Merz, Y. Miao, G. Monard, C. Nguyen, H. Nguyen, I. Omelyan, A. Onufriev, F. Pan, R. Qi, D.R. Roe, A. Roitberg, C. Sagui, S. Schott-Verdugo, J. Shen, C.L. Simmerling, J. Smith, R. Salomon-Ferrer, J. Swails, R.C. Walker, J. Wang, H. Wei, R.M. Wolf, X. Wu, L. Xiao, D.M. York and P.A. Kollman (2018), AMBER 2018, University of California, San Francisco.
(27) Wang, J.; Wolf, R. M.; Caldwell, J. W.; Kollman, P. A.; Case, D. A. Development and Testing of a General Amber Force Field. *Journal of Computational Chemistry* **2004**, *25* (9), 1157–1174. https://doi.org/10.1002/jcc.20035.
(28) Wang, J.; Wolf, R. M.; Caldwell, J. W.; Kollman, P. A.; Case, D. A. Junmei Wang, Romain M. Wolf, James W. Caldwell, Peter A. Kollman, and David A. Case, 'Development and Testing of a General Amber Force Field'Journal of Computational Chemistry(2004) 25(9) 1157–1174. *Journal of Computational Chemistry* **2005**, *26* (1), 114–114. https://doi.org/10.1002/jcc.20145.
(29) *MOPAC2016, James J. P. Stewart, Stewart Computational Chemistry, Colorado Springs, CO, USA, HTTP://OpenMOPAC.Net (2016).*
(30) Weinhold, F. Natural Bond Orbital Analysis: A Critical Overview of Relationships to Alternative Bonding Perspectives. *Journal of Computational Chemistry* **2012**, *33* (30), 2363–2379. https://doi.org/10.1002/jcc.23060.
(31) *NBO Version 3.1, E. D. Glendening, A. E. Reed, J. E. Carpenter, and F. Weinhold.*
(32) Gaussian 09, Revision A.02, M. J. Frisch, G. W. Trucks, H. B. Schlegel, G. E. Scuseria, M. A. Robb, J. R. Cheeseman, G. Scalmani, V. Barone, G. A. Petersson, H. Nakatsuji, X. Li, M. Caricato, A. Marenich, J. Bloino, B. G. Janesko, R. Gomperts, B. Mennucci, H.

P. Hratchian, J. V. Ortiz, A. F. Izmaylov, J. L. Sonnenberg, D. Williams-Young, F. Ding, F. Lipparini, F. Egidi, J. Goings, B. Peng, A. Petrone, T. Henderson, D. Ranasinghe, V. G. Zakrzewski, J. Gao, N. Rega, G. Zheng, W. Liang, M. Hada, M. Ehara, K. Toyota, R. Fukuda, J. Hasegawa, M. Ishida, T. Nakajima, Y. Honda, O. Kitao, H. Nakai, T. Vreven, K. Throssell, J. A. Montgomery, Jr., J. E. Peralta, F. Ogliaro, M. Bearpark, J. J. Heyd, E. Brothers, K. N. Kudin, V. N. Staroverov, T. Keith, R. Kobayashi, J. Normand, K. Raghavachari, A. Rendell, J. C. Burant, S. S. Iyengar, J. Tomasi, M. Cossi, J. M. Millam, M. Klene, C. Adamo, R. Cammi, J. W. Ochterski, R. L. Martin, K. Morokuma, O. Farkas, J. B. Foresman, and D. J. Fox, Gaussian, Inc., Wallingford CT, 2009.